DAAJ MARSHALL

THE INVESTIGATION OF TETHERED SATELLITE SYSTEM DYNAMICS

Contract NAS8-36160

Quarterly Report #4

For the period 15 May 1985 through 14 August 1985

Principal Investigator

Dr. Enrico Lorenzini

September 1985

Prepared for
National Aeronautics and Space Administration
Marshall Space Flight Center, Alabama 35812

Smithsonian Institution
Astrophysical Observatory
Cambridge, Massachusetts 02138

The Smithsonian Astrophysical Observatory
is a member of the
Harvard-Smithsonian Center for Astrophysics

(NASA-CR-176180) THE INVESTIGATION OF TETHERED SATELLITE SYSTEM DYNAMICS Quarterly Report, 15 May - 14 Aug. 1985 (Smithsonian Astrophysical Observatory) 71 p HC A04/MF A01 CSCL 22B

N85-35215

Unclas
G3/18 27413

THE INVESTIGATION OF TETHERED SATELLITE SYSTEM DYNAMICS

Contract NAS8-36160

Quarterly Report #4

For the period 15 May 1985 through 14 August 1985

Principal Investigator

Dr. Enrico Lorenzini

Co-Investigators

Mr. David A. Arnold
Dr. Mario D. Grossi
Dr. Gordon E. Gullahorn
Mr. William Harrold
Dr. Lee Parker

September 1985

Prepared for
National Aeronautics and Space Administration
Marshall Space Flight Center, Alabama 35812

Smithsonian Institution
Astrophysical Observatory
Cambridge, Massachusetts 02138

CONTENTS

CONTENTS (Cont.)

Abstract

The content of this Quarterly Report can be summarized as follows:

a) A brief study has been carried out on a retrieval rate control law with no angular feedback in order to investigate the dynamic response of the system.

b) The initial conditions for the computer code which simulates the satellite's rotational dynamics have been extended to the case of a generic orbit.

c) The model of the satellite thrusters has been modified in order to simulate a pulsed thrust (actual case), by making the SKYHOOK integrator suitable for dealing with delta functions without loosing computational efficiency.

d) Tether breaks have been simulated with the high resolution computer code SLACK3. Shuttle's maneuvers in order to avoid the recoiling tether have been tested.

e) The electric potential (in vacuo) around a severed conductive tether with insulator, in the case of a tether breakage at 20 km from the Shuttle, has been computed.

f) Preliminary evaluation of the electrodynamic hazards due to the breakage of the TSS electrodynamic tether in a plasma has been carried out.

1.0 INTRODUCTION

This is the fourth Quarterly Report submitted by SAO under contract NAS8-36160, "The Investigation of Tethered Satellite System Dynamics," Dr. Enrico Lorenzini, PI, and covers the period from 15 May 1985 through 14 August 1985.

2.0 TECHNICAL ACTIVITY DURING REPORTING PERIOD AND PROGRAM STATUS

2.1 Retrieval Using Rate Control

There are two basic types of retrieval control laws - tension control and rate control. The results reported in Quarterly Report #3 used tension control. Tension control laws are easily integrated into programs such as DUMBEL and SKYHOOK which integrate the motion in inertial coordinates given the forces on each mass point. In computer programs where the length of the wire is one of the integration variables, rate control laws can be easily implemented by using a first order differential equation for the length with the rate of change of length given by the control law. Such a system has a potential disadvantage in that there is no guarantee of positive tension in the wire since the radial acceleration and the tension are not involved in the integration. Rate control laws can be implemented in programs such as DUMBEL and SKYHOOK by including the natural length of the wire among the variables to be integrated. The rate of change of the length is specified by the control law. The tension in the wire is computed from the difference between the actual length and the natural length. In this system one can set the tension to zero if the actual length is less than the natural length so that there is no possibility of having negative

tension in the simulation. This method of simulation has a high fidelity to the actual physical situation where the reel motor pulls in wire, increasing the tension and accelerating the end mass.

The DUMBEL program already has a facility for integrating the natural length of the wire. Under a previous contract a model of a damper was added to the program in which the length of wire released by the damper reel is included as an integration variable. The program has been modified to use this variable for rate control in the retrieval mode of the program. For a perfect retrieval at a constant in-plane angle θ_c, the rate of change of wire length is

$$\dot{\ell} = - \alpha \ell \tag{1}$$

where

$$\alpha = \frac{3}{2} \omega_o \cos \theta_c \sin \theta_c \tag{2}$$

and ω_o = the orbital angular velocity.

A rate control retrieval mode has been added to the DUMBEL program using equation (1) to specify the rate of change of the natural length of the wire. A total of thirteen variables are integrated in the version without rotational dynamics. Six variables are required for the position and velocity of each mass and one for the variable giving the change in the natural length.

A test run has been done using equation (1) for retrieval in the DUMBEL program without rotation. The integration was started with equilibrium initial conditions consisting of a 7 m/sec retrieval velocity and a 12.1846 deg in-plane angle with θ_c = 12.1846 deg. The subsatellite was deployed downward on a 20 km tether. Figure 2.1.1 shows a plot of the in-plane angle vs. time for the first

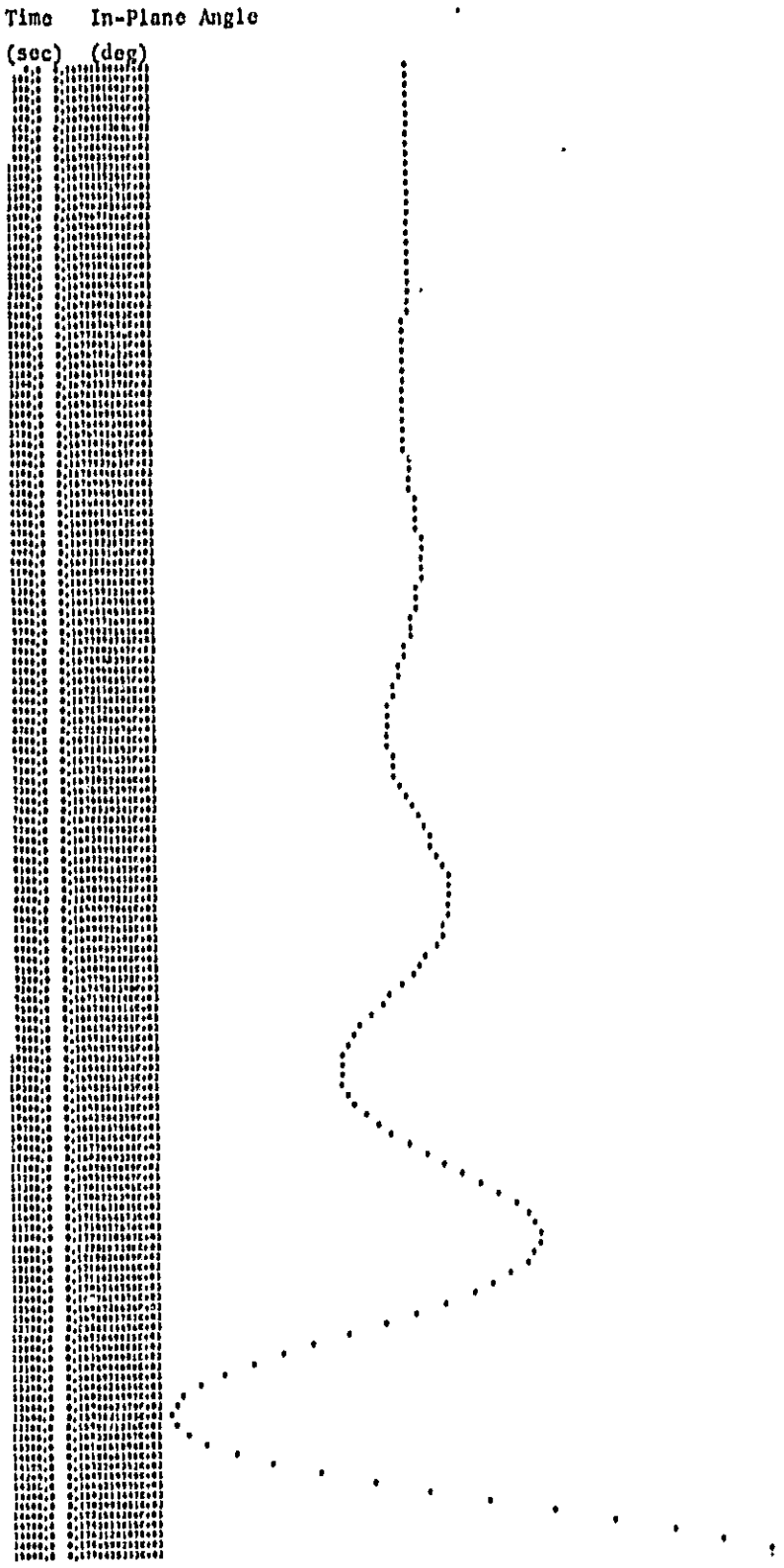

Figure 2.1.1. In-plane angle (deg) vs. time (sec) using rate control during retrieval of a satellite deployed downward on a 20 km tether.

15,000 seconds. The initial angle of 167.8152 is 12.1848 deg from the vertical position at 180 degrees. At 13,600 sec the subsatellite was 20.2179 degrees from the vertical. At 15,000 sec it is about to pass through the vertical at 180 degrees. As can be seen in the figure the in-plane librations are increasing in amplitude during the retrieval. The wire length at 15,000 seconds was 104 meters. The run was continued to 20,000 seconds and a wire length of 18 meters. The maximum in-plane deviation from the nominal retrieval angle was about 50 degrees. Although the run did not go unstable in the sense of having the subsatellite wrap-around the Shuttle, it is clear that this control law does not provide any damping to prevent the buildup of in-plane librations. Non-equilibrium initial conditions would presumably show more rapid development of librations. A damping term could be added to the rate control law using angle feedback. However the necessary information is not expected to be available to the reel control system on the first mission.

2.2 Initial Conditions For Inclined Orbits

The DUMBEL program has a facility for generating equilibrium initial conditions with the tether displaced from the vertical in the in-plane or out-of-plane directions. The original software was written in a simplified manner which could only be used for equatorial orbits. This facility has been updated by including an additional rotation to account for the orbital inclination. This facility will be needed to do simulations to study the effects of earth oblateness, etc. A short test run was done for a 28° inclination orbit with a 10 degree initial in-plane displacement and no out-of-plane displacement. Plots of the libration angles vs. time showed the proper behavior. The software changes were made in subroutine LAUNCH which

reads the libration angles and modifies the state vector.

The format of the output on DUMBEL has been changed to label each variable at each output point. The old format with a single heading at the beginning of the run was confusing to read on later pages.

2.3 Use Of Thrusters For Controlling Librations

2.3.1 Software Implementation -

The TSS is expected to have thrusters in the in-plane and out-of-plane directions which can be fired manually by commands from the Shuttle. In addition there will be an in-line thruster for use in maintaining wire tension during the final stages of retrieval. The thrust level for the transverse thrusters is 2.5 newtons and for the in-line thruster 2.0 newtons. The operator can enter a command for the thruster to fire at a certain time for a given duration not less than about 50 milliseconds. In contrast to the tension control algorithm which can operate in an automatic mode using data on length and length rate available to the deployer, the control of librations using thrusters must be done manually since angle information available in the cockpit is not transmitted to the deployer. Studies have been done to develop a procedure for using the thrusters to eliminate librations during retrieval.

The work done by a thruster is proportional to the velocity of the subsatellite at the time of firing. Therefore the most efficient technique is to fire the thruster near the time when the system is swinging through the vertical position and is at maximum swing velocity. The periods of the in-plane and out-of-plane librations are about 3206 and 2776 seconds respectively at 400 km altitude. The times for one quarter of a cycle are 801 and 694 seconds

respectively. In order to keep the firing near the maximum velocity and upper limit of 100 seconds has been used for the firing time.

If the velocity is low enough, the swinging motion can be stopped with one firing. The firing interval required can be computed, at least approximately, from the amplitude and period of the oscillation. Suppose the oscillation is given by the equation:

$$x = A \sin (\omega t) \tag{3}$$

where x is the displacement of the subsatellite from the local vertical, A is the maximum displacement and ω is the frequency of the libration. For the in-plane component, the frequency is $\sqrt{3}\,\omega_o$, and for the out-of-plane 2 ω_o where ω_o is the orbital frequency. The velocity is

$$\dot{x} = A\,\omega \cos (\omega t)$$

The maximum velocity is

$$v = A\,\omega \tag{4}$$

The time required to stop the motion is

$$T = v/a \tag{5}$$

where a is the deceleration. If the mass of the subsatellite is m and the thruster force is F then the acceleration is

$$a = F/m \tag{6}$$

Combining equations 4, 5, and 6 gives

$$T = m\ A\ \omega/F \tag{7}$$

The computer implementation of the firing commands must take into account the way the numerical integrator works. The integrator uses variable step size to maintain the integration accuracy requested by the user. The user must supply a subroutine that computes the forces on each mass as a function of the extrapolated state vector computed by the integrator. Before taking a step, the integrator will try various step sizes to see how large a step can be taken and still maintain the required accuracy. The times given to the subroutine supplied by the user are therefore not monotonic and the subroutine must be prepared to deal with random input times. The stepsize varies greatly depending on the nature of the function being integrated. At a discontinuity the stepsize may be as small at 10^{-7} seconds. During periods when the behavior is smooth the stepsize may be 25 seconds or more.

A subroutine has been written to generate firing intervals for the thrusters. The subroutine operates in three modes. In the first mode the subroutine tests the libration amplitude to see if it has exceeded the deadband specified by a parameter. If the amplitude of the libration has exceeded the deadband a flag is set to search for the next maximum in the libration angle. At each call, the amplitude is compared to that on the previous call and the time and amplitude saved if the value is larger. If it has been more than 1/8 of the libration period since the amplitude has increased the subroutine sets a flag indicating that a maximum has been reached and the program goes to the next mode. In the third mode the program searches for a zero crossing. This is done by looking for a change in sign of the amplitude of the libration. Because of

the way the integrator works the time of the zero crossing may be as much as 25 seconds away from the first time a change in sign is detected. In this preliminary version of the software the difference has been ignored. The subroutine simply takes the first time there is a sign change and sets this as the on time for the thruster. The firing interval is computed from equation 7 using the maximum amplitude A determined in mode 2 of the subroutine. If the time T is greater than 100 seconds the firing interval T is set to 100 seconds. This system does not center the firing time around the zero crossing and the on time may be off by an amount not exceeding the integrator stepsize.

2.3.2 Retrieval Simulation Using Thrusters -

As a first test of the thruster control software the tether was given an initial in-plane displacement of 30 degrees. The in-plane thrusters were fired each time the subsatellite crossed the local vertical. The simulation was run for 10,400 seconds with no retrieval. The subsatellite was deployed downward on a 20 km tether. The thruster fired for 100 second intervals beginning at 859, 2568, 4270, and 5968 seconds. The firings were effective in reducing the amplitude of the librations. The approximate times and amplitudes of the maximum libration angles are listed in Table 2.3.1.

Table 2.3.1

Maximum libration angles vs. time.

T (sec)	Amplitude (km)
0.	+ 10.000
1700.	- 9.768
3400.	+ 9.535
5100.	- 9.305
6800.	+ 9.077
8500.	- 8.850

In the second test run, the tether was given an initial out-of-plane displacement of 10°. The out-of-plane thrusters were fired for 100 second intervals each time the out-of-plane displacement went through zero. The amplitude of the out-of-plane displacement decreased at each thruster firing. However, the decrease was not sufficient to keep the out-of-plane angle from increasing during the retrieval. At around 8900 seconds, the radial component went from negative (downward deployment) to positive (upward deployment). The tether length at that time was about one kilometer. From that point on, the subsatellite was being retrieved from above. The run was terminated at 19,500 seconds at a tether length of about 47 meters. At the beginning of the run, the firing time computed from equation 7 was 1729 seconds. The computed firing time decreased after each thruster firing but by more than 100 seconds the largest decrease being about 337 seconds at around the time the system flipped to upward deployment. Since the amplitude of the libration became very large, the tension control law probably provided significant damping of the out-of-plane component since the coupling between the radial and out-of-plane components increases with amplitude. Toward the end of the run the firing interval dropped below the integration stepsize of 25 seconds, and the program started skipping over the firings, so that there was no further decrease in the out-of-plane component.

The plot of the in-plane angle in the previous runs was not satisfactory in the case of downward deployment. The angle is 180° near the vertical, but the usual normalization is from -180° to +180° so that there is a change of 360° as the in-plane angle crosses the local vertical. The normalization was changed to be from -90° to +90° when the cosine of the angle is positive and 90° to 270° when the cosine of the angle is negative.

In the next test run, the system was given ann initial out-of-plane displacement of 3° and the out-of-plane thrusters were used during retrieval.

The thruster were fired for 100 seconds at each zero crossing until the firing time required to stop the libration went below 100 seconds. The firing times and the firing interval required to stop the libration are listed in Table 2.3.2 for each zero crossing.

Table 2.3.2

Start Time for Each Thruster Firing and

Firing Interval Required to Stop the Libration

Thruster Start Time	Computed Firing Duration
660.1	521.1
1997.9	425.8
3432.5	345.3
4821.3	234.4
6208.3	136.5
7479.1	35.3

The computed firing duration decreases by roughly 100 seconds on each zero crossing. The run was terminated at 7513.7 seconds because the integration stepsize became prohibitively small. In an attempt to understand the source of the problem, the run was repeated with output intervals of 1 second starting at 7480 seconds and continuing to the time at which the integration failed. The output interval on the original run was 100 seconds which did not give enough time resolution to study what was happening. Plotting the out-of-plane displacement vs. time showed that the libration velocity was going to zero at the point where the problem occurred. From Table 2.3.2 we see that the libration was computed to go to zero at 7479.1 + 35.3 = 7514.4 seconds. If the thruster had fired for the whole 35.3 seconds the velocity would have been cancelled and slightly reversed. Since the thruster must fire in the direction opposite to the velocity, the thrust direction must be reversed if the sign of

the velocity changes. This reversal of sign caused the integration to get hung up because the thruster started rapidly reversing direction at the point where the velocity went to zero.

In order to solve the problem of the thruster reversing direction, the program was changed to terminate the thruster firing when the magnitude of the libration velocity falls below a prescribed limit. The next run was done with a lower limit of 1 cm/sec on the libration velocity. The same initial out-of-plane angle of 3° was used. The thruster fired five times for 100 seconds. The computed firing intervals for each activation were 521, 425, 345, 234, and 136 seconds. On the sixth zero crossing the computed firing interval was 35.2 seconds. The thruster fired for 32.4 seconds before shutting off at the 1 cm/sec limit. Since the acceleration provided by the thruster is F/m = 2.5 newtons/550 kg = .0045 m/sec^2, it would have required another 2.3 seconds to stop the motion, for a total firing time of 34.6 seconds. Successive short firings seem to have been either missed by the integrator or turned off by the 1 cm/sec lower velocity limit. The run was ended at 20,000 seconds with a final wire length of 23.4 meters.

The above run was repeated, lowering the velocity limit to .01 cm/sec. There were 5 firings of 100 seconds followed by a 34.56 second firing (computed interval 35.28 sec). The seventh scheduled firing of 3.49 seconds was skipped by the integrator. The eighth firing computed as 2.08 seconds was performed and lasted 2.03 seconds before being terminated by the 0.1 cm/sec lower velocity limit. The ninth scheduled firing of .31 seconds was also skipped by the integrator. The run ended at 20,000 seconds and the final wire length was 23.5 meters. The out-of-plane libration had an amplitude of only 1.3 degrees at the end of the retrieval.

Starting the thruster firing at the time the system crosses the vertical has the disadvantage that the firing interval is not symmetrically placed around the time of maximum velocity. The center of the firing should be at the point of maximum velocity. The subroutine has therefore been changed to compute the approximate time of the zero crossing by adding one quarter of the libration period to the time of the last maximum. The firing interval can then be centered about the predicted time of the zero crossing. This procedure should work well on the last firing by leaving the system stopped at the zero crossing. If the velocity of the subsatellite is v, and the time required to stop the subsatellite with the thruster is dt, the satellite should travel a distance dtv/2 during the deceleration period. Since the thruster is fired at a time dt/2 before the zero crossing it should be at a distance vdt/2 from the zero crossing when the thruster fires and should arrive at the zero crossing with zero velocity. Stopping the subsatellite at a point other than the zero crossing does not eliminate the libration since the point at which it stops becomes the maximum swing angle for the subsequent oscillations.

The next computer run was done with the same initial conditions but using the predicted time of the zero crossing to set the firing time. The start time was set equal to the predicted time of the zero crossing minus the firing interval of 100 seconds (the program should have used 50 seconds - half the firing interval). The run was satisfactory with the exception of the error noted and the fact that short firings were still being skipped by the integrator.

The next computer run incorporated the following changes. The start time was corrected to be the time of the zero crossing minus half the firing interval to center the firing time around the zero crossing. In order to check the actual time of the zero crossing, a section of code was added to compare the

successive values of the displacements from the vertical and print out the first time where a change of sign occurred (this being accurate only to within the stepsize used by the integrator). The code was later changed to interpolate to find the zero crossing. The final change was to rewrite the code governing the start and stop times for the thruster to prevent the integrator from skipping over firing intervals shorter than the integration stepsize. To do this the software was changed to save and make available to the thruster control subroutine the time of the last step taken by the integrator. The logic was then split into three sections depending on whether the time of the last step was before, during, or after the commanded firing interval. In case 1, the last step is before the start time. The integrator may ask for the forces at any later time up to the maximum allowable stepsize. If the time is before the start time, the thruster force is of course zero. During the firing interval the thruster is on. The critical change is for times after the stop time for the thruster. In case 1 the program returns an "on" value for the thruster. This has the effect of preventing the integrator from skipping over the thruster firing. The integrator will try shorter stepsizes until it finds the start time for the thruster. In case 2, the last step is during the firing interval. If the time requested is before the stop time the thruster is on, and if it is after the stop time it is off. For case 3, the last step is after the stop time and the thruster is always off.

The results of the computer run were as follows. Table 2.3.3 lists the start time, zero crossing time, end time, and firing interval (actual and computed) for each of the thruster firings. In the intervals before and after the last firing at 15,592 seconds, the out-of-plane angle was within the deadband of .01 radians. Since the amplitude of the out-of-plane oscillation is constant (as measured in length units) the angular amplitude keeps increasing as

the wire length decreases. Therefore, any non-zero oscillation will eventually exceed an angular deadband if the retrieval continues long enough. The stepsize was about 40 seconds at the time of the last firing, but the new software prevented the integrator from skipping over the firings.

Table 2.3.3

Start Time, Zero Crossing Time, End Time and Firing Interval for Retrieval with an Initial Out-Of-Plane Angle of 3 Degrees and Out-Of-Plane Thruster Firings. Times are in seconds.

T_{DEC}	T_{ZERO}	T_{END}	ΔT	ΔT (COMPUTED)
644	652	744	100	521
1950	1987	2050	100	424
3359	3462	3459	100	343
4811	4881	4911	100	231
6243	6408	6343	100	132
7803	8465	7832	29	29
	9889			
	11325			
	12756			
	14186			
15592	16064	15593	1	1
	17494			
	18924			

In the runs described up to this point it has been noticed that the predicted times of the zero crossings do not seem to be very accurate. In the run just described the zero crossings listed in Table 2.3.3 are obviously not centered in the firing interval. The prediction is computed from the time of the largest amplitude which is accurate only to within the stepsize used by the integrator. For the 100 sec firing, the crossings occurred 8,37,103,70 and 165 seconds after start time. For the sixth firing of 29.4 seconds duration, the velocity was reduced to a small value and the next crossing was 663 seconds after the start time. In other words, the point where the thruster stopped firing became the maximum of the next libration. The seventh firing at 15592 seconds also reduced the velocity to a low value and the next crossing was 472

seconds after the start time. The extrapolated time of the zero crossing without a thruster firing was 15616 seconds which is 24 seconds after the start time of the seventh firing.

The thruster firings obviously alter the dynamics of the librations so that it is difficult to draw any conclusions about the natural periods from thruster runs. A run has been done with retrieval but no thruster to look at the periods of the librations. The system was given an initial out-of-plane angle of 3 degrees and no in-plane angle. For greater resolution the simulation was run with output every 25 seconds rather than 100 seconds as in previous runs. The approximate time of the maxima were tabulated for both the out-of-plane displacement and the out-of-plane angle. The amplitude of the out-of-plane displacement was nearly constant during the retrieval, with some decrease toward the end as the angle became large enough to provide coupling with the radial variable. The time for each quarter cycle was reasonable constant at around 710 seconds. The theoretical value for small oscillation is 694 seconds. For the out-of-plane angle the quarter cycle from the zero crossing to maximum angle was systematically larger (about 795 seconds) than the quarter cycle from the maximum angle to the zero crossing (about 650 seconds). The numbers were somewhat crudely calculated but the effect is unmistakable. There were fluctuations in the times for each quarter cycle of the out-of-plane displacement (as measured in length units) sufficient to explain the errors observed previously in predicting the zero crossings. Coupling with the in-plane component may provide an explanation but the effect was not carefully studied.

In order to see just the effect of out-of-plane to in-plane coupling a run was done with an initial out-of-plane angle of 20 degrees and no thrusters or retrieval. The out-of-plane oscillation induced an in-plane libration of about

3 degrees. A quarter cycle of the out-of-plane was around 705 seconds and there was a fluctuation of about 10 seconds. It appears that various factors such as thruster firings, reeling operations, and coupling between modes may complicate the dynamics of the tether librations so that the zero crossings are difficult to predict exactly.

As an alternative to trying to predict the time of the zero crossing, the thruster control algorithm has been revised to use the tether displacement for setting the start time of the thruster firings. In this mode, the peak velocity computed from equation (4) is multiplied by half the firing time from equation (5) to determine at what point to start the thruster. When the tether reaches that position the firing start and stop times are set. A 20,000 second run has been done with output every 100 seconds. The tether is given an initial out-of-plane displacement of 3 degrees. The tension control algorithm is used to control the in-plane angle and the thruster to control the out-of-plane during retrieval. In order to better analyze the periods of the librations the plotting program has been revised to calculate the times of the extrema and zero crossings by interpolation between the output data points. For the zero crossing, a linear interpolation is used. For the maxima and minima a quadratic is fitted to the 3 points near the extremum and the time of the extremum computed analytically from the equation for the quadratic. The accuracy of this procedure depends on the interval between the output points on the plot file. Table 2.3.4 lists the start time, zero crossing time, end time, and firing interval (actual and computed) for each thruster firing. For the 100 second firings, the zero crossing occurs 50, 54, 57, 59 and 72 seconds after the start time. For the last firing of 27 seconds duration the zero crossing is 371 seconds after the firing. This is because the motion was essentially neutralized by the firing. For the first firing the zero crossing is well

centered in the firing interval. The zero crossings occur successively later in the interval as the libration amplitude and velocity decrease with each thruster firing.

Table 2.3.4

Start Time, Zero Crossing Time, End Time, Firing Interval (Actual and Computed), and Time of the Last Extremum for the Out-Of-Plane Displacement. Times are in Seconds.

T_{BEG}	T_{CROSS}	T_{END}	ΔT	ΔT (Computed)	T_{MAX}
604	654	704	100	521	0
1945	1999	2045	100	423	1311
3408	3465	3508	100	342	2733
4818	4877	4919	100	230	4168
6259	6331	6359	100	113	5583
7727	8098	7754	27	27	7024
	9531				
	10959				
	12389				
	13819				
	15249				
	16679				
	18109				
	19539				

The zero crossing times in Table 2.3.4 are from the printout of the program and have been determined by interpolation between steps taken by the integrator. These steps are shorter than the output interval of 100 seconds. In Table 2.3.5 the results from the plotting program are tabulated. This program uses the output at 100 second intervals for interpolation. Table 2.3.5a is the out-of-plane displacement and Table 2.3.5b is the out-of-plane angle. The zero crossing times differ somewhat between Table 2.3.4 and Table 2.3.5 because of the different time intervals used for interpolation. Table 2.3.4 should be more accurate for this quantity. The largest difference is for the fifth zero crossing where the dynamics is strongly affected by the thruster firing. The times of the extrema given in Table 2.3.4 and Table 2.3.5a differ by a few

seconds. The values in Table 2.3.4 are not interpolated and are probably less accurate. The times for a quarter period given in the last column of Tables 2.3.5a and 2.3.5b show substantial fluctuations. In Table 2.3.5a the fluctuations are only during the period of thruster firings. After the last firing the length of a quarter cycle is consistently close to 715 seconds. For the out-of-plane angle, the quarter cycles are asymmetric after the end of the thruster firings. It takes about 786 seconds to go from the zero crossing to maximum angle, but only about 643 seconds to go from the maximum angle to the zero crossing. Apparently the displacement is simpler to model than the angle during retrieval.

Table 2.3.5a

Times (sec) of the Extrema and Zero Crossings for the Out-Of-Plane Displacement. The Last Column Lists the Time for Each Quarter Cycle.

T_{MIN}	T_{CROSS}	T_{MAX}	T_{DIFF}
0			
	657		657
		1315	658
	1999		684
2728			729
	3469		742
		4166	697
	4881		715
5889			707
	6349		761
		7029	680
	8098		1069
8814			716
	9531		717
		10245	714
	10959		714
11674			715
	12390		715
		13105	715
	13819		715
14534			715
	15249		715
		15964	715
	16679		715
17394			715
	18109		715
		18824	715
	19529		715

Table 2.3.5b

Times (sec) of the Extrema and Zero Crossings for the Out-Of-Plane Angle. The Last Column Lists the Time for Each Quarter Cycle.

T_{MIN}	T_{CROSS}	T_{MAX}	T_{DIFF}
0			
	657		657
		1352	695
	1999		647
2815			816
	3468		653
		4227	759
	4881		653
5665			785
	6348		683
		7098	749
	8098		1000
8887			788
	9530		644
		10315	785
	10958		643
11746			788
	12389		643
		13176	786
	13819		643
14605			786
	15248		643
		16035	787
	16679		643
17465			787
	18109		643
		18895	786
	19538		643

Figure 2.3.1 shows plots of the results for the run above. Part a) shows the wire length vs. time starting from 20 km and going to 23 meters. The subsatellite is initially stationary and slight deviations from a perfect exponential retrieval can be seen in the plot resulting from the action of the tension control law. Part b) of the figure shows the tension as a function of time starting from 5.6×10^6 dynes and going down to 4.5×10^3 dynes. The action of the control law is evident in the plot. Plot c) shows the in-plane displacement vs. time. Part d) shows the in-plane angle vs. time. Under the action of the tension control law the in-plane angle approaches the equilibrium angle of 167.82 degrees with the amplitude of the angular oscillations decreasing by about a factor of two on each cycle. The angle of 167.82 degrees is 12.18 degrees from the vertical at 180 degrees. Part e) shows the out-of-plane displacement vs. time. The amplitude of the oscillation is reduced by the thruster firings at each zero crossing. After the sixth firing the remaining oscillations are not visible on this scale. Part f) shows the out-of-plane angle vs. time. Although the amplitude of the out-of-plane displacement is always decreasing as seen in part e), the out-of-plane angle can increase with time as the length of the wire decreases. The angle is still growing after the first four thruster firings but is nearly eliminated by the last two firings. The small remaining oscillation produces a noticeable angular oscillation by the end of the run. The amplitude was within the deadband used of .01 radians (.57 degrees) so there were no further thruster firings. Part g) shows the out-of-plane vs. in-plane displacement. The line starts at the lower left corner with an out-of-plane displacement but no in-plane displacement. The line ends in the bottom center of the plot with virtually no out-of-plane displacement and a continually decreasing in-plane displacement. Part h) shows the in-plane angle vs. out-of-plane angle. The line starts at the upper left corner with an in-plane angle of 180 degrees (local vertical) and an out-of-

Figure Captions

Figure 2.3.1. Retrieval of a subsatellite deployed downward on a 20 km tether using tension control and out-of-plane thrusters.

a) Wire length (cm) vs. time (sec)

b) Tension (dynes) vs. time (sec)

c) In-plane displacement (cm) vs. time (sec)

d) In-plane angle (deg) vs. time (sec)

e) Out-of-plane displacement (cm) vs. time (sec)

f) Out-of-plane angle (deg) vs. time (sec)

g) In-plane displacement (cm) vs. out-of-plane displacement (cm), 0-20000 sec.

h) In-plane angle (deg) vs. out-of-plane angle (deg), 0-20000 sec.

i) In-plane angle (deg) vs. out-of-plane angle (deg), 7800-20000 sec.

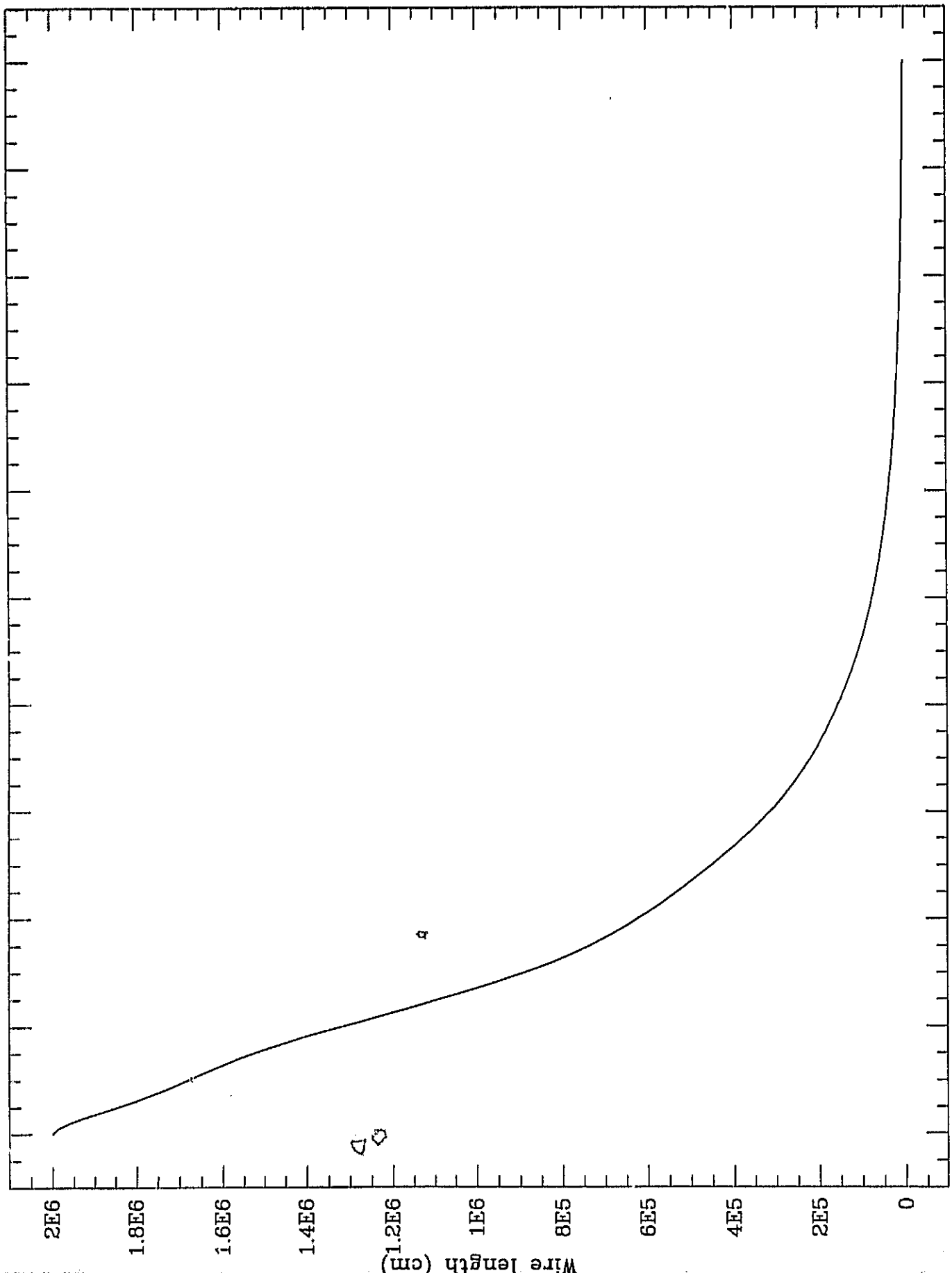
Wire Length (cm)
2E6
1.8E6
1.6E6
1.4E6
1.2E6
1E6
8E5
6E5
4E5
2E5
0
0
2000
4000
6000
8000
10000
12000
14000
16000
18000
20000
Time (sec)

Figure 2.3.1a

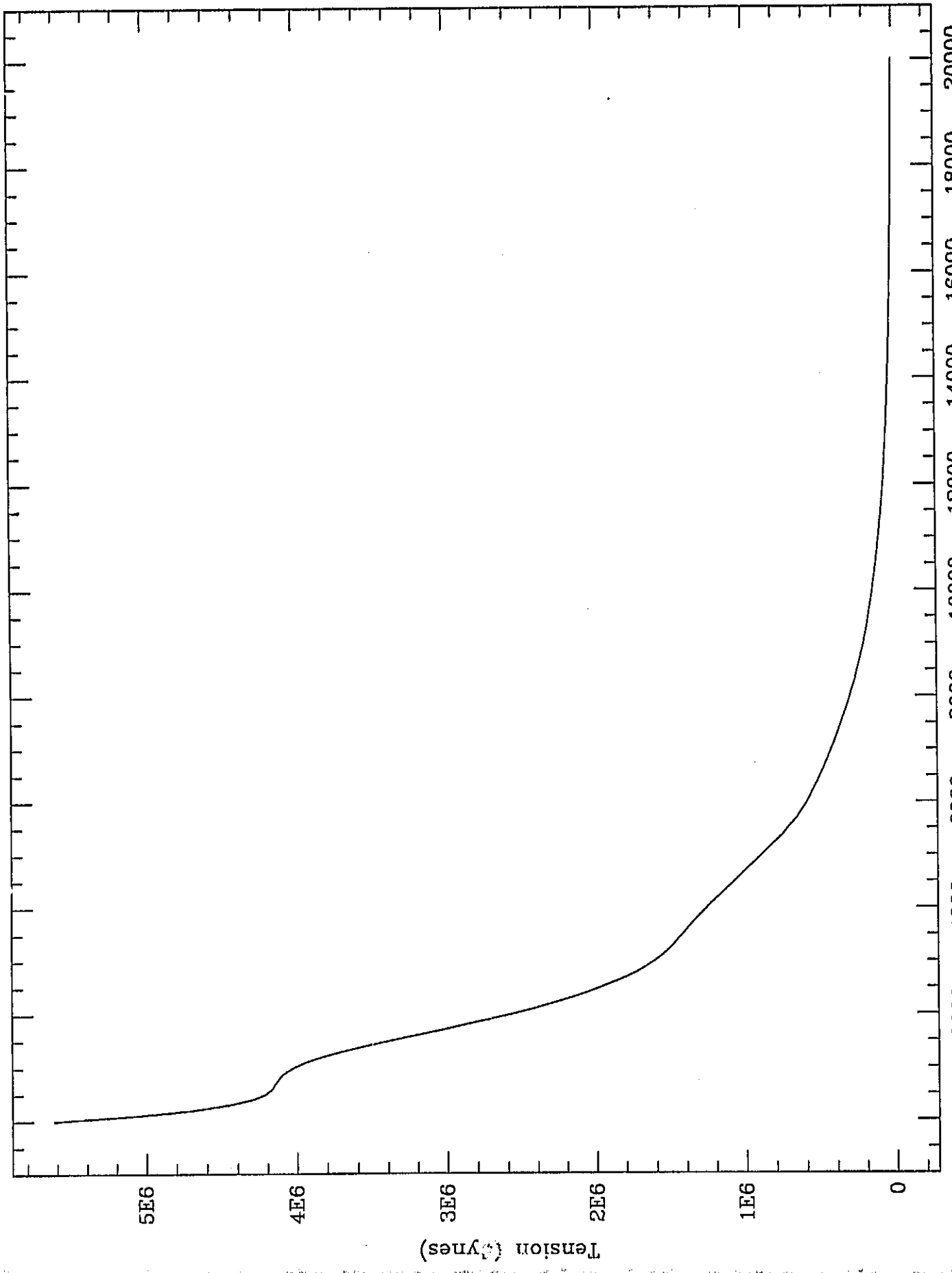
Tension (dynes)
5E6
4E6
3E6
2E6
1E6
0
0
2000
4000
6000
8000
10000
12000
14000
16000
18000
20000
Time (sec)

Figure 2.3.1b

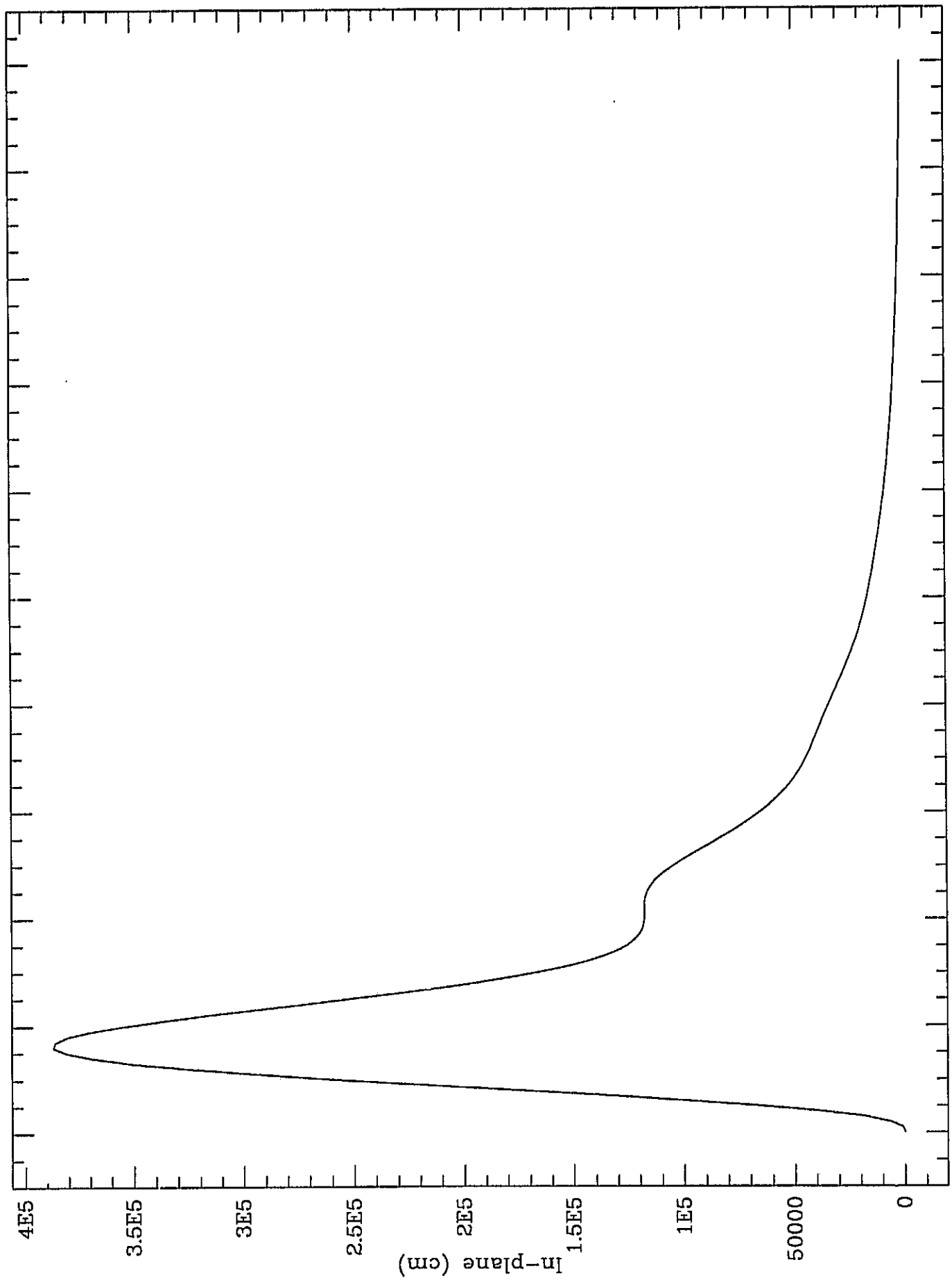
4E5
3.5E5
3E5
2.5E5
2E5
1.5E5
1E5
50000
0
In-plane (cm)
0
2000
4000
6000
8000
10000
12000
14000
16000
18000
20000
Time (sec)

Figure 2.3.1c

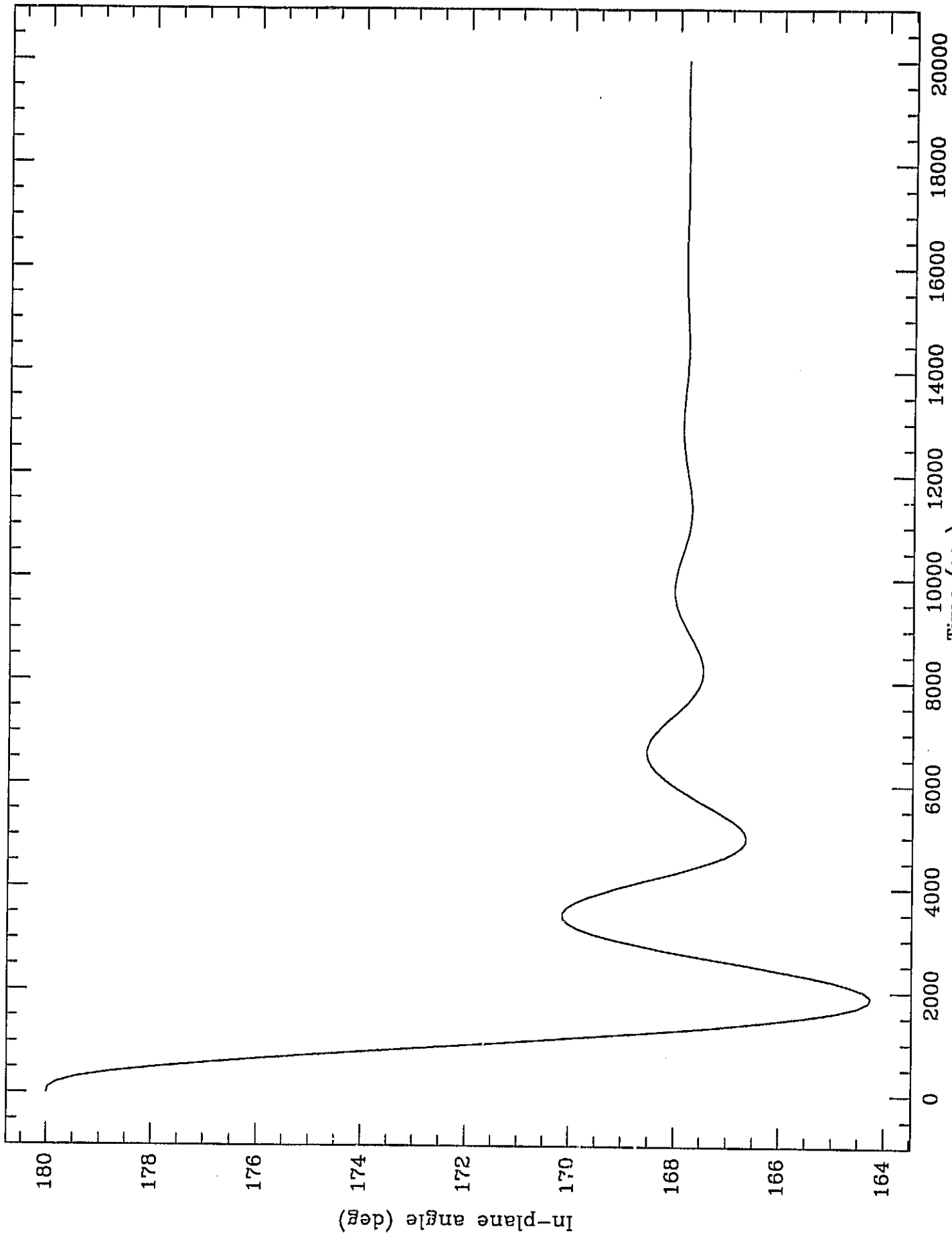
In-plane angle (deg)
180
178
176
174
172
170
168
166
164
0
2000
4000
6000
8000
10000
12000
14000
16000
18000
20000
Time (sec)

Figure 2.3.1d

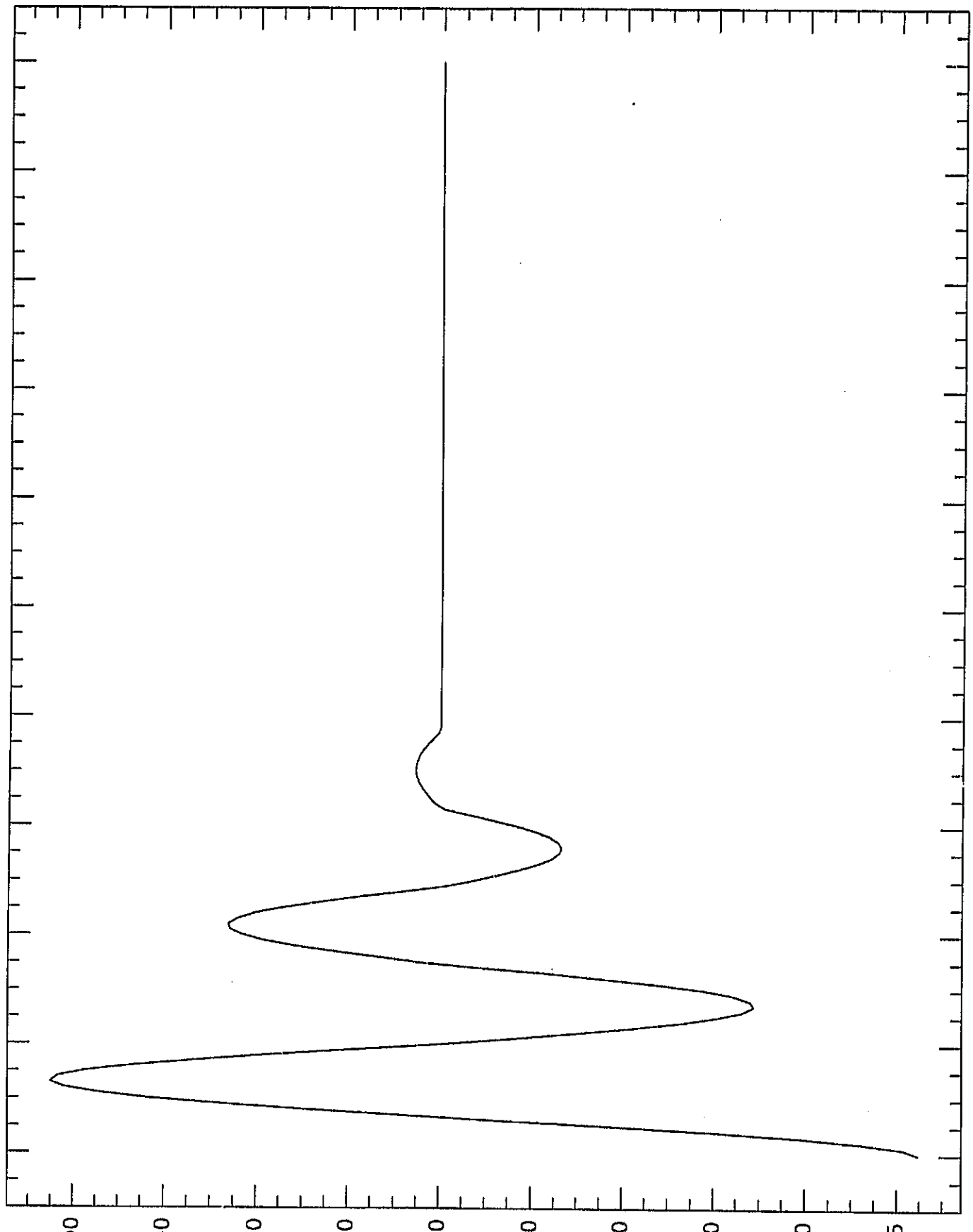
80000
60000
40000
20000
0
−20000
−40000
−60000
−80000
−1E5
Out−of−plane (cm)
0
2000
4000
6000
8000
10000
12000
14000
16000
18000
20000
Time (sec)

Figure 2.3.1e

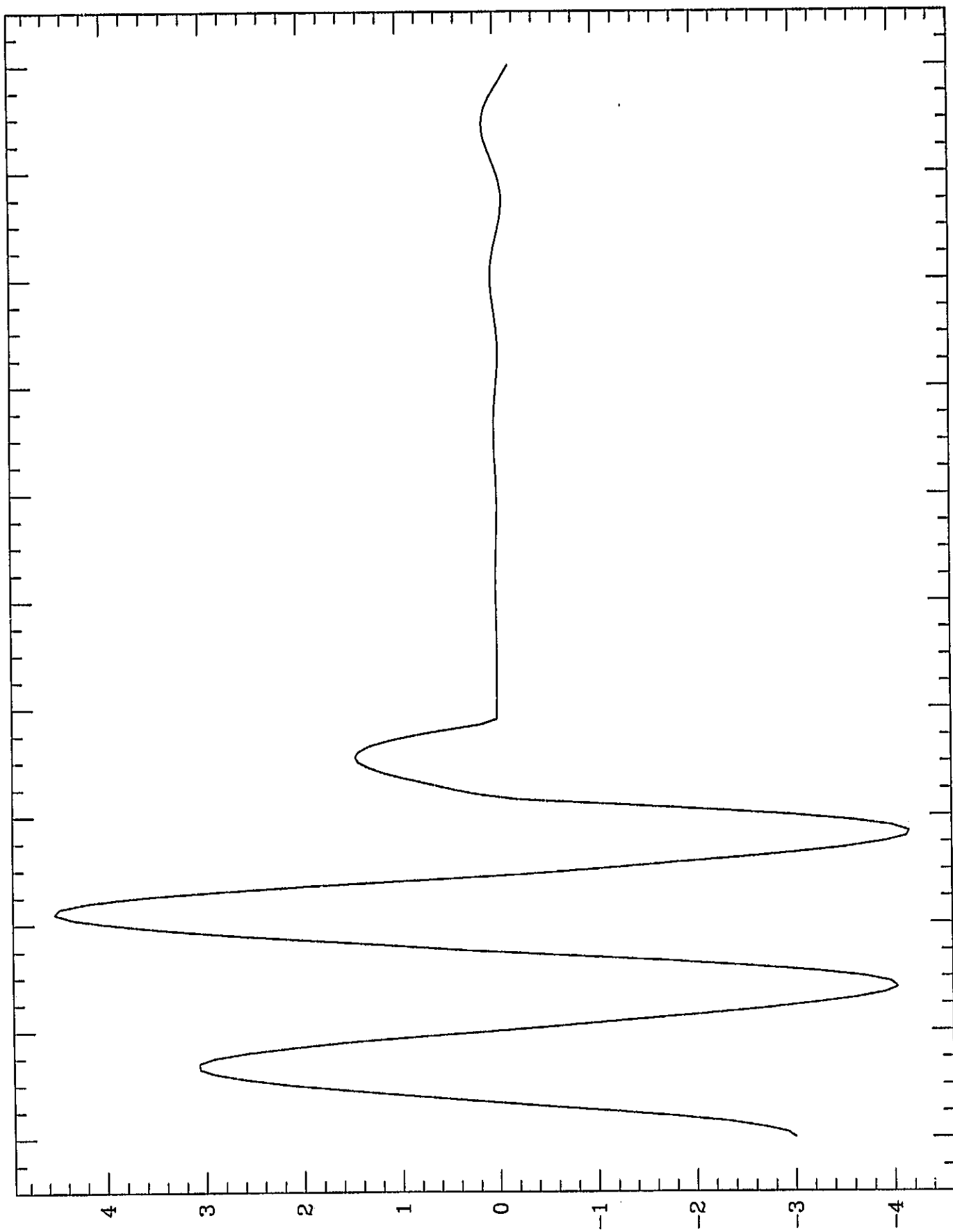
Out-of-plane angle (deg)
4
3
2
1
0
-1
-2
-3
-4
0
2000
4000
6000
8000
10000
12000
14000
16000
18000
20000
Time (sec)

Figure 2.3.1f

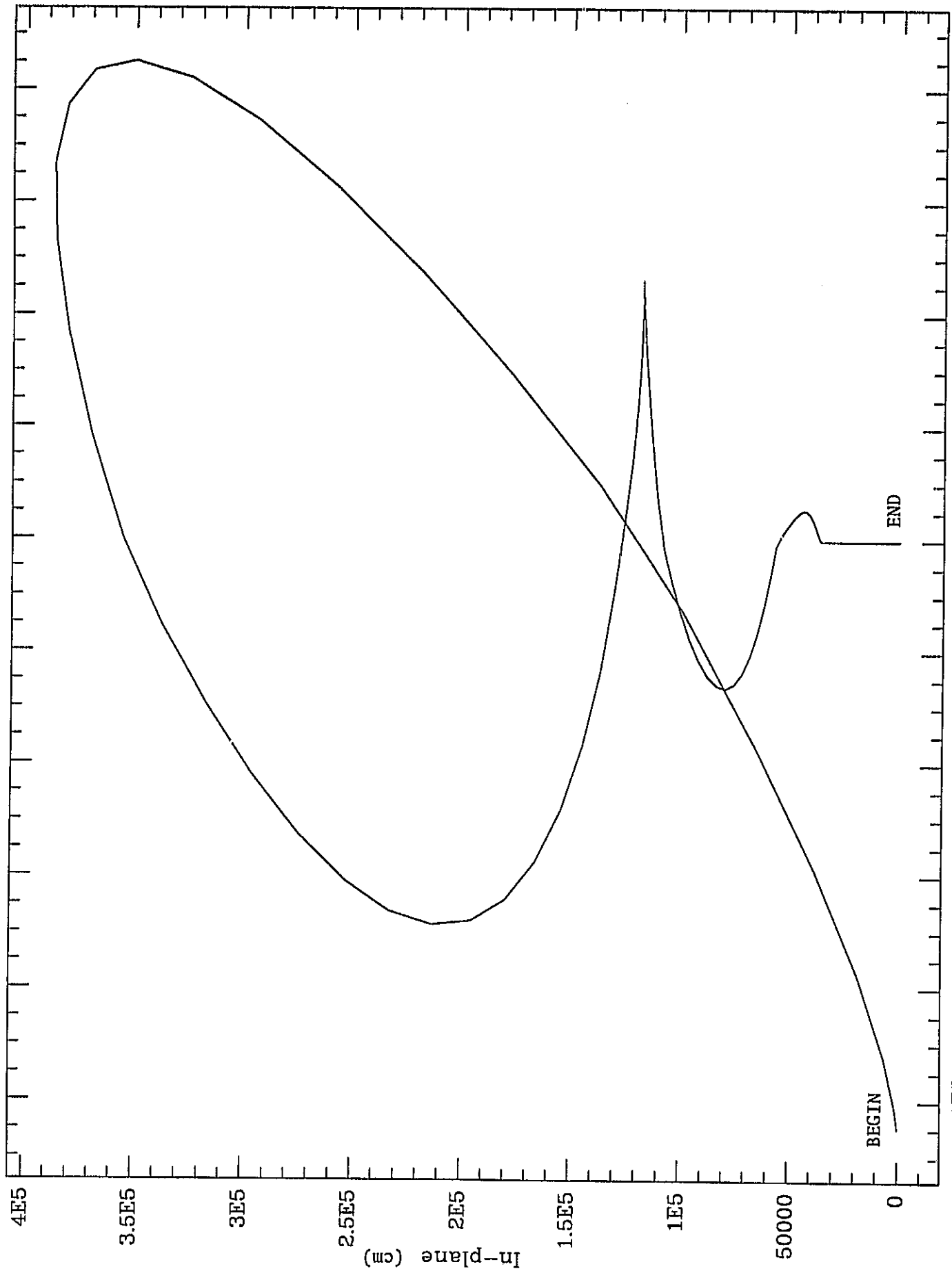
4E5
3.5E5
3E5
2.5E5
2E5
1.5E5
1E5
50000
0
In-plane (cm)
-1E5
-80000
-60000
-40000
-20000
0
20000
40000
60000
80000
Out-of-plane (cm)
END
BEGIN

Figure 2.3.1g

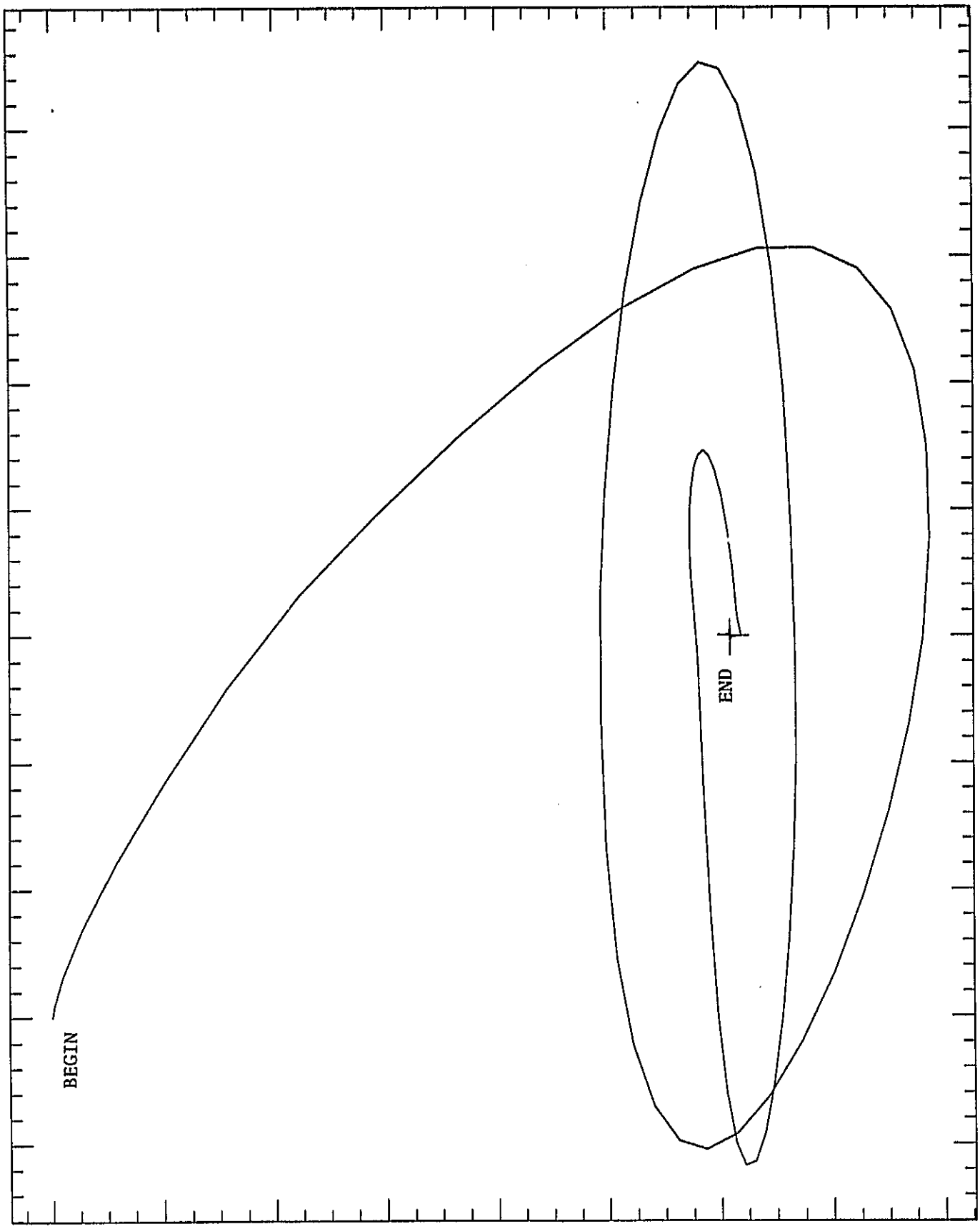
BEGIN
END
In-plane angle (deg)
180
178
176
174
172
170
168
166
164
Out-of-plane angle (deg)
4
3
2
1
0
-1
-2
-3
-4

Figure 2.3.1h

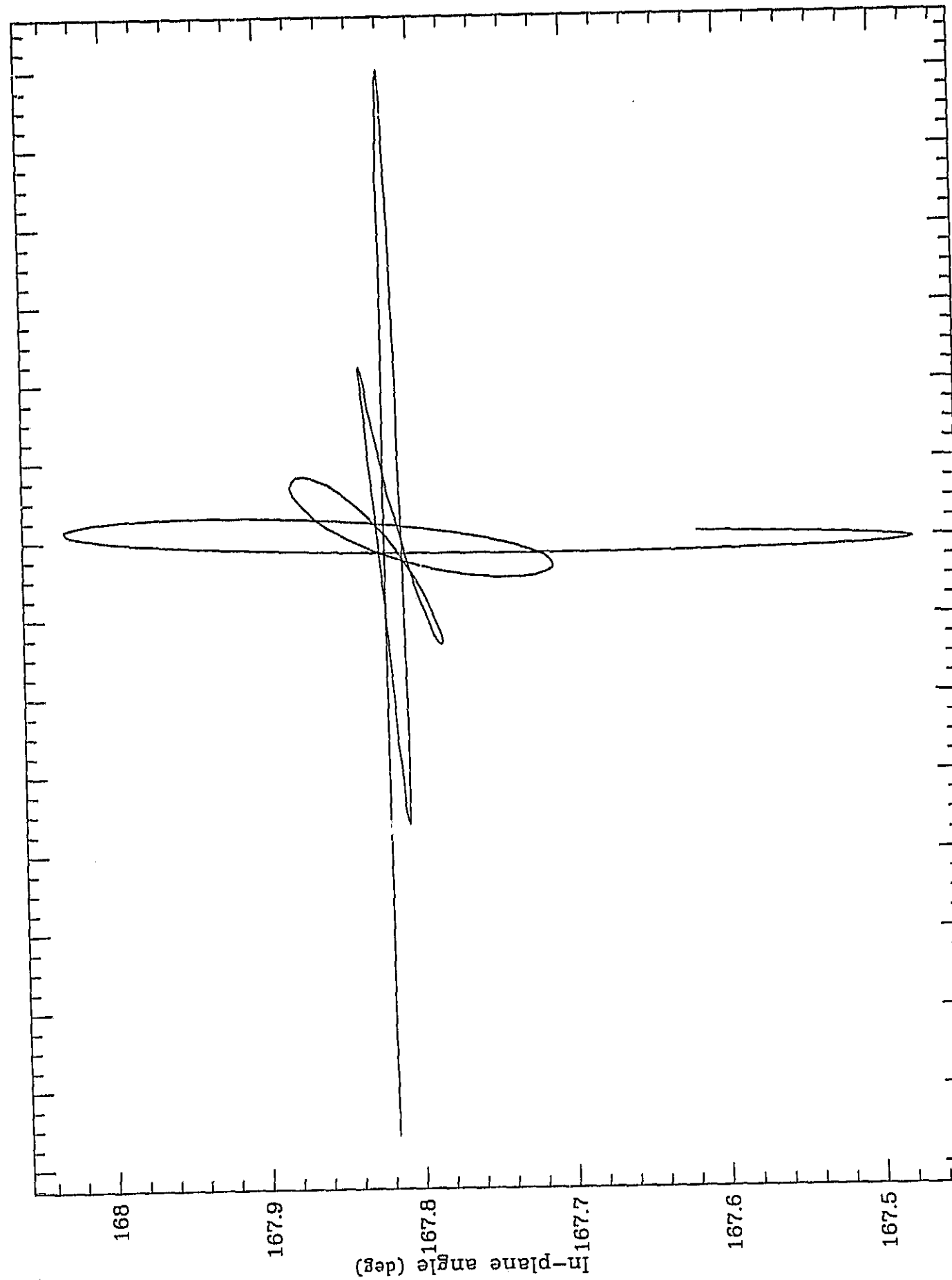
In-plane angle (deg)
168
167.9
167.8
167.7
167.6
167.5
-.16
-.14
-.12
-.1
-.08
-.06
-.04
-.02
0
.02
.04
.06
.08
.1
.12
Out-of-plane angle (deg)

Figure 2.3.1i

plane angle of -3 degrees. The in-plane angle converges to 167.82 degrees and the out-of-plane angle approaches zero because of the thruster firings. Part i) is a blow-up of the last part of Figure 2.3.1h after the last thruster firing. This plot covers the time period 7800 seconds to 20,000 seconds. The line begins in the lower center of the plot with an oscillation that is primarily in the in-plane direction. The sixth thruster firing has largely eliminated the out-of-plane oscillation. The tension control law continues to damp the in-plane angular oscillations, but the out-of-plane angle increases because the out-of-plane oscillation has a fixed amplitude (in centimeters) and the length of the wire is continually decreasing. At the end of the simulation the oscillation is primarily in the out-of-plane direction.

2.4 Slack Tether Studies

During the reporting period SAO has modified SLACK3 to include avoidance maneuvers using Shuttle thrusters and run several simulations. A number of approximate criteria were also developed to estimate the total *possible* downfall of tether onto the Shuttle under various circumstances.

2.4.1 SLACK3: Shuttle Thruster Avoidance Maneuvers -

The SLACK3 input and setup routine was modified to accept a Shuttle thruster maneuver with parameters: direction (specified as pitch and roll angles); acceleration (cm/sec^2); initial delay (sec) and cutoff (sec). These parameters are passed in commons to BOOM, the subroutine generating the deployment boom tip's position; the Shuttle center of mass position is computed, to which are added any rotation maneuver and boom vibration. Experience led us to add an option to produce plot output relative to the instantaneous Shuttle center of mass, rather than the coordinate origin at the original Shuttle c.m., passing the c.m. position in commons to the output routine. This is, after all, what we wish to see and otherwise the overall system motion dominates the tether/Shuttle motion, confusing the plot.

We derive a Shuttle acceleration adequate for our purposes as follows: The Shuttle has four forward and three reverse thrusters, with thrusts in the range 800-900 pounds thrust; use an average of 850. Now, one "pound thrust" in everyday units becomes (1 pound) x (1/2 kilogram/pound) x (g = 10m/sec^2) = 5 Newton. Thus one thruster produces about 850 x 5 = 4×10^3 N thrust. Taking the mass of the Shuttle as 10^5 kg, the acceleration produced per thruster is then $4 \times 10^3 / 10^5 = 4 \times 10^{-2}$ m/sec^2 = 4 cm/sec^2.

To examine the utility of various thruster maneuvers in avoiding the recoil of a broken tether we took one of the cases presented in the last quarterly report and added several different maneuvers. The case used was that of a 20 km tether cut at 1 km (see Figure 2.3.1 of the previous quarterly). This was in some sense the most "dangerous" of the cases considered: high recoil velocity (220 cm/sec) due to full deployment, with a long remnant. (Longer remnants, e.g. 20 km cut at 10 km, might prove more dangerous or less amenable to

avoidance, due to the way in which the tether does not simply fly by the Shuttle but "bounces" up and down by a fraction of a kilometer, but as detailed in the last report these are difficult to simulate due to the tether coming into full tension.)

The avoidance maneuvers all burned three thrusters, i.e. had an acceleration of 12 cm/sec^2. The thrust was initiated at 5 seconds after the break; this allows (2.2 m/sec) x (5 sec) = 11 meters of tether to downfall onto the Shuttle before initiating avoidance, but some delay was regarded as inevitable to avoid false alarms. The two other parameters each had two possible values, leading to four cases: The direction was either straight forward or 90° to one side; the acceleration was either cut off after 20 seconds (i.e. at t = 25) or simply allowed to run. The 20 sec cutoff was chosen to give a 20 meter displacement (about 2/3 Shuttle length) at cutoff: distance = $\frac{1}{2}at^2 = 0.03t^2$ meter.

The results are shown in Figures 2.4.1 to 2.4.4.

The two runs with no thruster cutoff terminate on excess computation time after having completed only a part of the requested simulation (Figures 2.4.1 and 2.4.2). This is probably due to the tether's trying to come into full tension, which as discussed in Section 2.3.1.3 of the last report, is a difficult situation for SLACK3 to cope with: it attempts many closely spaced bounces, and may simply fail. Effectively we are placing an artificial gravitational field on the tether by constantly accelerating the Shuttle.

Overall, the runs with out-of-plane thrust are more successful in avoiding the tether. Thrust in this direction eliminates the complications of drag and Coriolis forces. Figure 2.4.3 demonstrates that a brief impulse, 20 seconds of thrust, is adequate for initial avoidance of the vast majority of the tether.

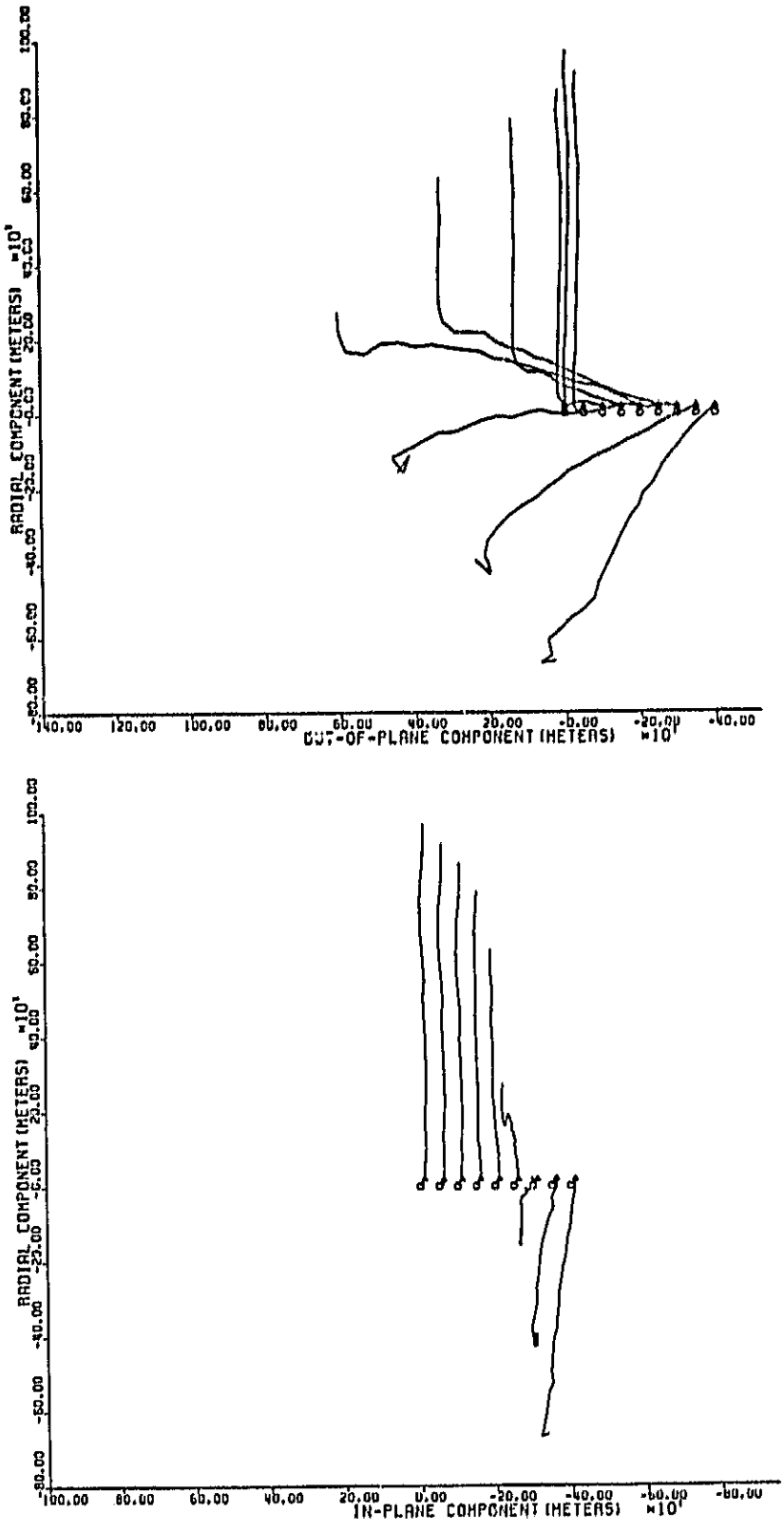

Figure 2.4.1. Thruster avoidance maneuver. Original 20 km tether cut at 1 km, resulting in recoil velocity of 2.2 m/sec. Three thrusters, producing acceleration of 0.12 m/sec, initiated at 5 seconds after the break. Directed perpendicular to orbital plane, with no thruster cutoff. Output at 25 second intervals, total run of 200 seconds. Model has 25 tether mass points.

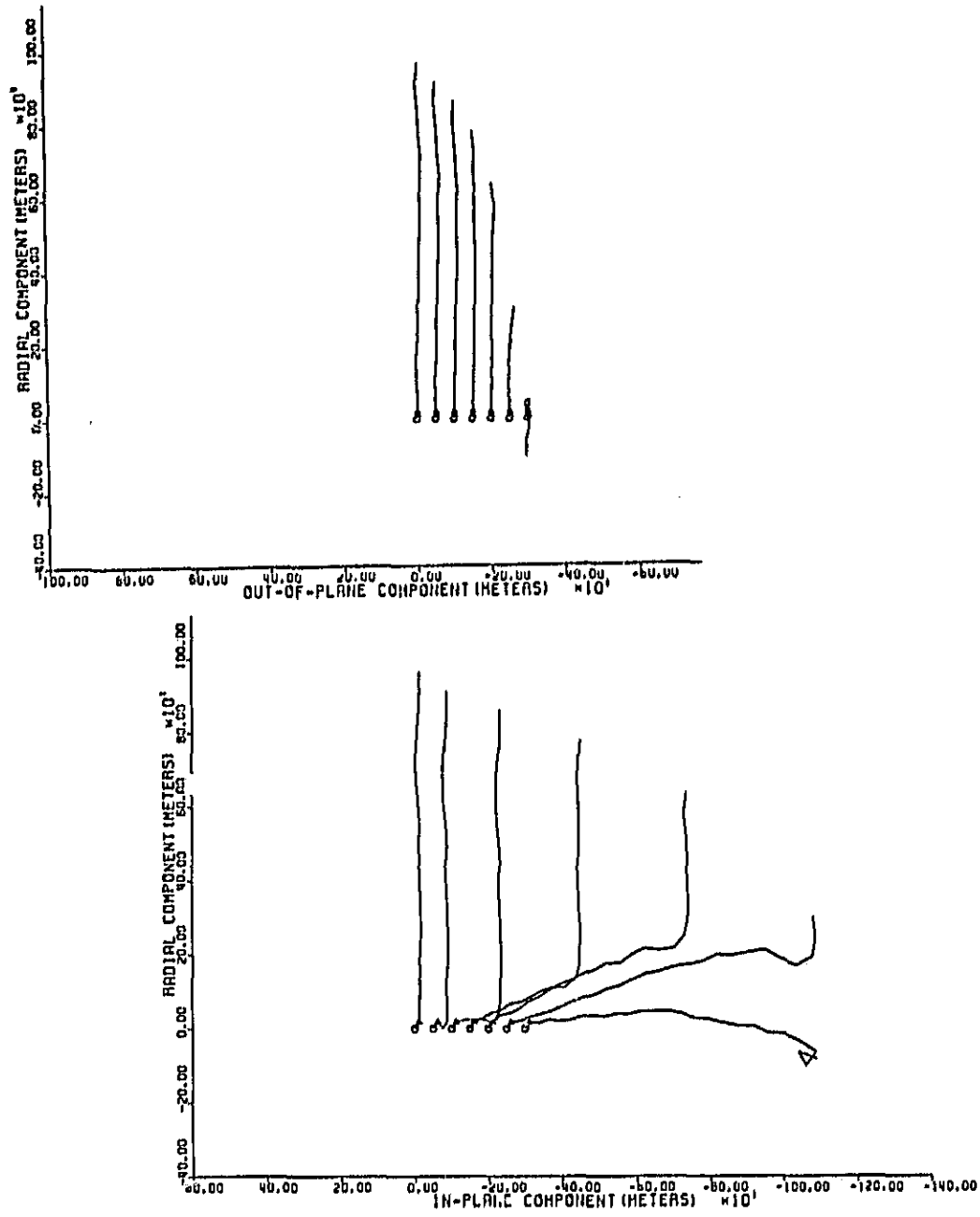

Figure 2.4.2. As for Fig. 2.4.1, except: Thrusters directed along-orbit, no cutoff, total run of 125 seconds.

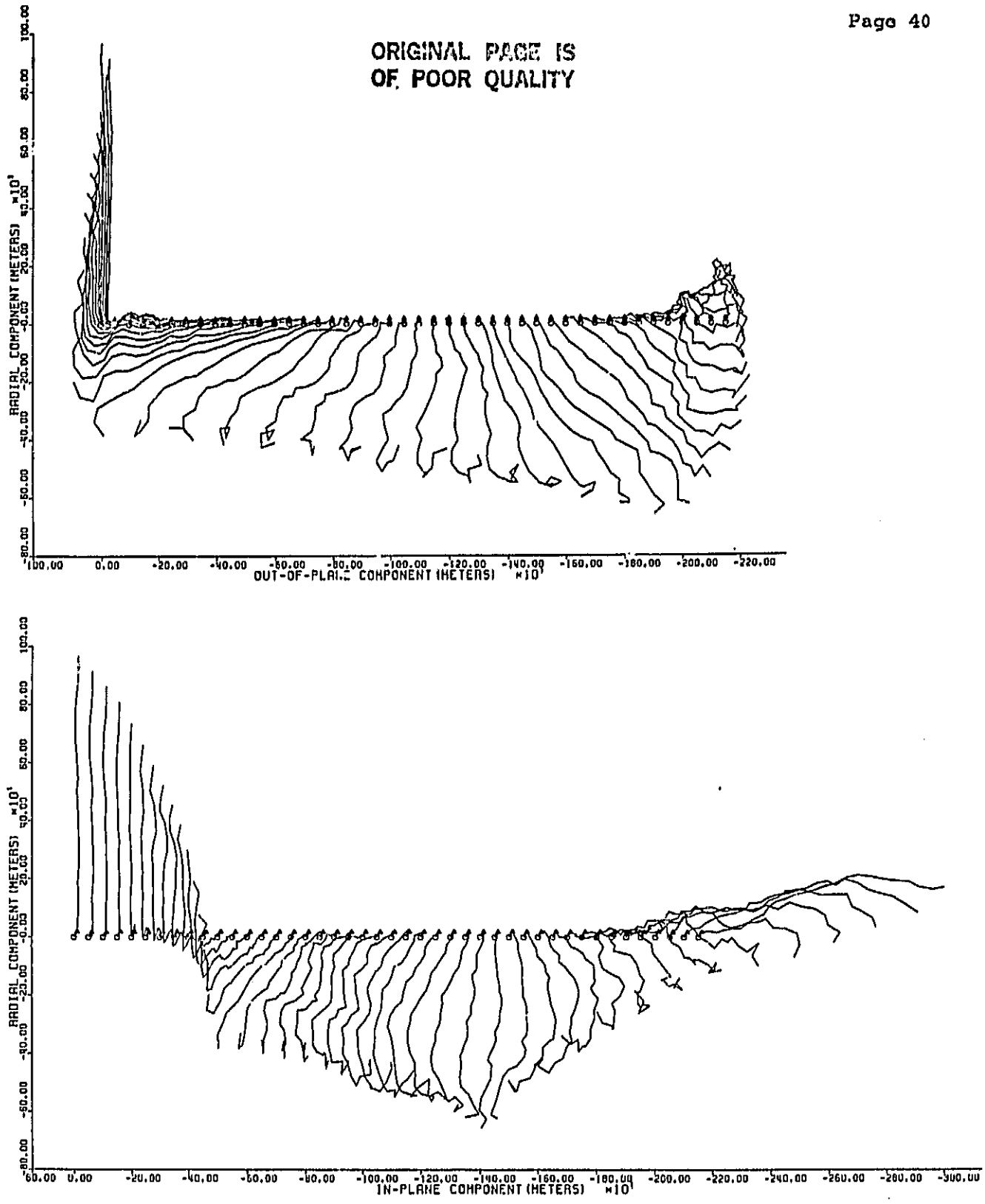

Figure 2.4.3. As for Fig. 2.4.1, except: Thrusters directed perpendicular to orbital plane, cutoff after 20 second burn, total run of 1075 seconds.

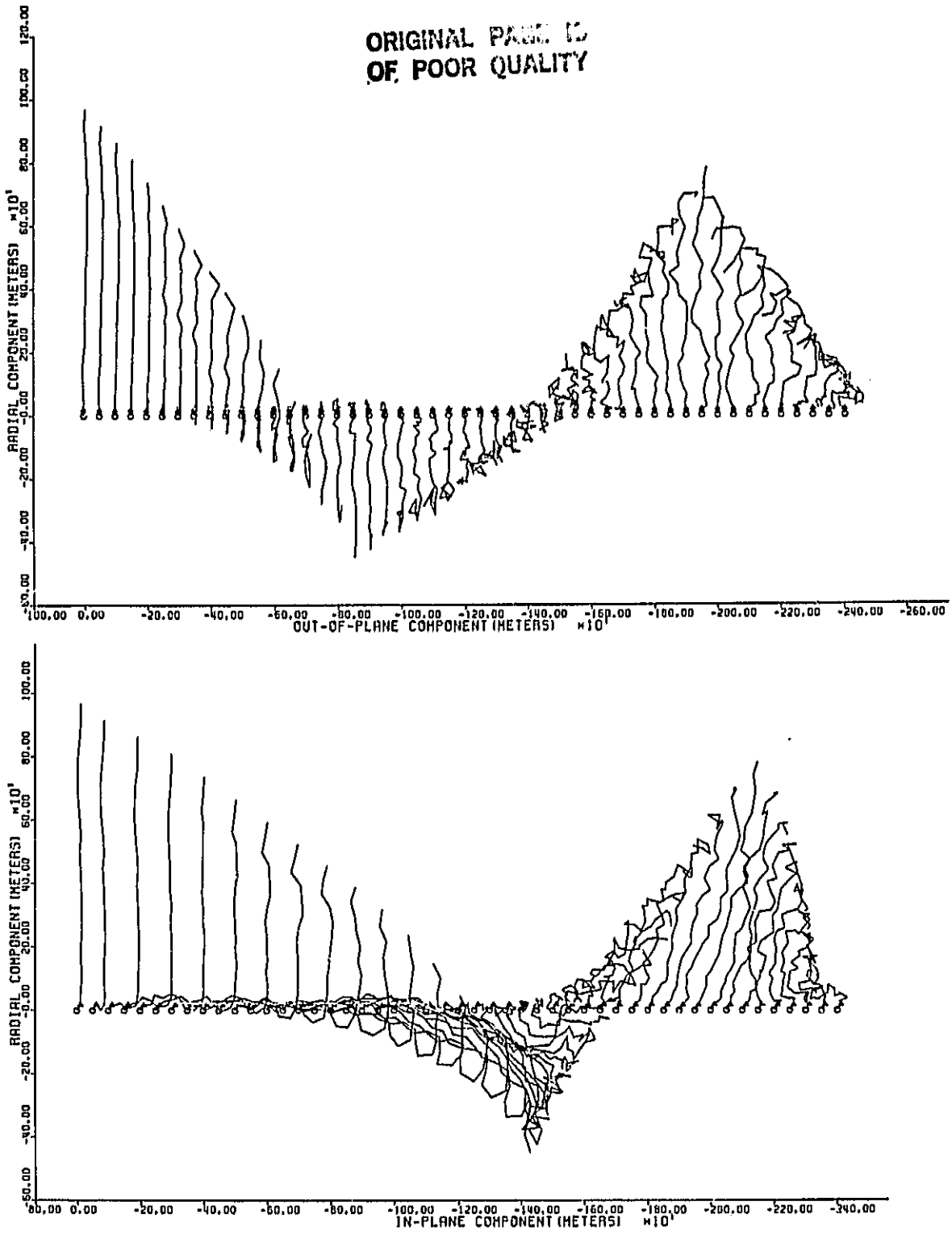

Figure 2.4.4. As for Fig. 2.4.1, except: Thrusters directed along-orbit, cutoff after 20 second burn, total run of 1200 seconds.

(It seems unlikely that we can totally avoid downfall onto the Shuttle; what is desirable, and possibly achievable, is to minimize this downfall and avoid wrap-around.) However, after recoiling by the Shuttle and bouncing at full extension in the downward direction, the tether tip "whips" around and on rebounding the tether comes around the other side of the Shuttle, wrapping around it. A more complicated maneuver appears necessary to avoid this wrap-around (the fact that it happens in the out-of-plane direction as well as in-plane indicates that we cannot simply modify the initial burn parameters). Two possibilities are: (1) when the tether is fully extended below, apply another brief burn (in a combination of in-plane and out-of-plane directions) to match the Shuttle velocity with the tether tip velocity, with a bit extra for avoidance, and (2) rotate the Shuttle to match the average wrap-around angular velocity.

2.4.2 High Resolution Loss-Of-Tension Model -

There has been no effort on this task in the reporting period.

2.4.3 Analytical Studies Of The Slack Tether Problem -

There has been no effort for this contract on this task during the reporting period.

SAO has acquired a separate contract with Martin Marietta Corporation (MMC) for theoretical and innovative modeling studies of the detensioned tether. The majority of the analytical studies will now be performed under the MMC contract (while lumped mass studies such as SLACK3 will continue under the current NASA contract). Specific applications to electrodynamic tether safety studies may be made when appropriate under the current contract and will be reported on at that

time.

2.4.4 Feasibility Arguments For Tether Impact On Shuttle -

In the last quarterly report, Figure 2.4.2, we saw that not all severed tethers will recoil fully to the Shuttle, even ignoring the Coriolis and drag forces which displace them from the direct path. In the particular case illustrated there, a 20 km tether cut at 10 km merely "bounced" toward the Shuttle and away by a half kilometer or so.

In this section, we present some crude, "back-of-the-envelope" arguments addressed to questions such as: Will the tether go slack at all? How much of the tether might conceivably impact on the Shuttle?

Throughout, we assume that the tether is initially deployed straight up (or down) and is in equilibrium. The following notation is used:

ℓ	=	original tether length
r	=	remnant tether length (after cut)
D	=	downfall tether length (possible impact on Shuttle)
m	=	subsatellite mass
μ	=	tether mass per unit length
EA	=	tether elasticity
c	=	tether speed of sound (= $\sqrt{EA/\mu}$)
Ω	=	orbital angular velocity

In general we make the crudest possible assumptions; e.g. we use only the subsatellite mass, and not the tether mass, when computing the gravity gradient force before the break. We also assume throughout that the amount of tether stretch is small compared to the natural length. In numerically evaluating the formulae, we use $\Omega = 1.2 \times 10^{-3}$ sec^{-1}, m = 500 kg, $\mu = 1.1 \times 10^{-2}$ kg/m, EA = 0.6×10^{5} kg m/sec^2 (c = 2.34×10^{3} m/sec).

For our first criterion, we ask the question "Is there enough stored elastic energy in the tether remnant at the moment of the cut for the entire tether to move far enough against the gravity gradient field to become detensioned?" . The significance of this question is based on the observation that the wave of slackening proceeds along the tether from the point at which it was cut, as seen in Section 2.2.4 of Quarterly Report #2 with the high resolution loss of tension model. That simulation did not include gravity gradient forces, but in their presence we should expect that the sharp tension profile would become smoother as the wave propagates toward the tether; as the gravity gradient potential energy dominates the elastic energy, the detensioning wave will at some point merely be reducing the tension to some positive value (rather than zero) by the time it reaches the Shuttle.

To quantify this argument we need two energies: The stored elastic energy in the remnant, E_{EL}. The energy, E_{SL}, needed to move against the gravity gradient force from the initial configuration to one in which each element of the tether is just barely detensioned. For E_{EL}, we assume a massless tether; this simplifies the tension calculation and also means that each tether element is stretched by the same amount. The tether spring constant of the segment which will become the remnant is then $k = EA/r$ and the gravity gradient force is $F = 3\Omega^2 \ell m$. The total stretch of the remnant portion is then $\Delta r = F/k = \frac{3\Omega^2 m \ell r}{EA}$. Considering this segment as a simple spring, the stored elastic energy is then $E_{EL} = \frac{1}{2}k(\Delta r)^2 = \frac{9}{2}\frac{\Omega^4 m^2}{EA} r\ell^2$. To compute E_{SL}, we first compute the energy required to raise each mass element of the tether from its position in the initial configuration to that in the "barely slack" configuration. Let s be the natural (detensioned) length along the tether from the Shuttle attachment to a given element. The tether has been <u>uniformly</u> stretched by an amount $\epsilon = \Delta r/r = 3\Omega^2 m\ell/EA$. Consider an element of length ds and mass $dm = \mu ds$ at coordinate s.

It was originally displaced by an amount ϵs, and now must move by this amount against the gravity gradient force, which is $F(s) = 3\Omega^2 s dm$. The energy required is thus $dE = (\epsilon s)F(s) = 3\epsilon\Omega^2\mu s^2 ds$, where we have used $dm = \mu ds$. The total energy required to move from the initial configuration to the zero-tension configuration is then obtained by integrating dE from s=0 to s=r and substituting for ϵ: $E_{SL} = 3\,\frac{\Omega^4 m\mu}{EA}\, r^3\, \ell$. Note the r^3 dependence of E_{SL} (in a uniform gravity field it would be r^2) and the simple r^1 dependence of E_{EL}; this implies that for a given original length ℓ, the energy required to go completely slack will be negligible compared to the stored elastic energy for short remnants, but as the remnant length is increased the elastic energy will at some point be unable to overcome the gravity gradient forces. This cross-over point is found by equating the two energies:

$$r = \sqrt{\frac{3}{2}\frac{m}{\mu}\,\ell} \qquad (1)$$

$$= \sqrt{75\text{km}\;\ell}$$

For shorter remnant lengths, the tether has enough elastic energy to go completely slack; for longer remnants, there is not enough elastic energy to go completely slack. (A short remnant, however, is not guaranteed to go slack.) As discussed above, if a remnant does not go completely slack, it seems likely that the portion near the Shuttle will remain taut. Note that any remnant from a tether with original length less than 75 km will have the energy to go slack, since the critical remnant length will be longer than the original length.

Our next two criteria respond to the question "Assuming the tether becomes slack, how much of the tether could conceivably impact on the Shuttle?" In both cases we ignore drag and are only concerned with whether or not such impact is,

in some sense, energetically allowable.

For criterion number two, we imagine that at the moment the tether goes completely slack it is cut up into infinitesimal mass elements. These elements will all be moving toward the Shuttle with a uniform velocity given by $\frac{1}{2}\mu r v^2 = E_{EL}$, leading to $v = 3\Omega^2 m\ell/\mu c$ where $c \equiv \sqrt{EA/\mu}$. In a Shuttle-centered coordinate system with the x-axis pointing radially outward and the y-axis forward along orbit, the governing equations for a given mass are:

$$\ddot{x} = 3\Omega^3 x + 2\Omega\dot{y}$$
$$\ddot{y} = -2\Omega\dot{x}$$

which can be solved (see Section 4.2.1 of the Final Report for NAS8-35036, "Investigation of Electrodynamic Stabilization and Control of Long Orbiting Tethers," PI G. Colombo) to give

$$x(\tau) = s\ (4 - 3\cos(\tau)) - V\sin(\tau)$$
$$y(\tau) = 2V\ (1 - \cos(\tau)) + 6s\ (\sin(\tau) - \tau)$$

for a mass element with initial conditions $x(0) = s$, $y(0) = 0$, $\dot{x}(0) = -v = -\Omega V$, $\dot{y}(0) = 0$; τ is a dimensionless time, $\tau = \Omega t$.

We are interested in which elements cross the Shuttle's orbit, i.e. have $x(\tau) < 0$ for some τ. The maximal s for given recoil velocity V which allows this is the downfall D. $x(\tau) = 0$ can be written

$$4 - 3\cos(\tau) = \frac{V}{s}\sin(\tau)$$

and by finding the value of V/s for which the curve on the left is just tangent

to the curve on the right we achieve the downfall D. This is

$$\frac{V}{D} = \sqrt{7}$$

which gives rise to

$$D = \frac{3\Omega m}{\sqrt{7}\ \mu\ c}\ \ell\ = 0.026\ \ell \qquad (2)$$

Note that this estimate of the downfall is independent of where the tether is cut.

For the third criterion, we assume that the elastic energy E_{EL} is much greater than needed to achieve full slackness. Once slack, we assume that the tether moves toward the Shuttle uniformly, and that any tether impacting on the Shuttle is retained. We neglect drag and Coriolis forces, so that the tether continues to fall directly on the Shuttle. How far can the entire tether move toward the Shuttle against the gravity gradient force before exhausting the stored elastic energy which has been converted to kinetic energy? The potential energy of a tether of length ℓ in the gravity gradient field is $E_{CG}(L) = -\frac{1}{2}\Omega^2\mu\ \ell^3$. We then wish to find the downfall D from a tether cut at length r such that $E_{EL} = E_{CG}(r-D) - E_{CG}(r)$. If we assume that the downfall is only a small part of the remnant length, then we have

$$D = 3\ \frac{\Omega^2 m^2}{\mu EA}\ \frac{\ell^2}{r} \qquad (3)$$

$$= 1.6 \times 10^{-3}\ \frac{\ell^2}{r}$$

Now this criterion, in contrast to the free orbit criterion (2), depends on both

the original length ℓ and the remnant length r. We can put two limits on this: first, let the tether be cut at its full length, $r = \ell$, which gives directly:

$$D = 0.0016\ \ell$$

and second, after noting that the downfall increases as the remnant length decreases, suppose that the entire remnant becomes downfall, leading to $D^2 = 0.0016\ \ell^2$ or

$$D = 0.040\ \ell$$

This latter estimate agrees well with that of (2) numerically, and indeed is only different by a factor of $\sqrt{3/7}$.

How do these compare with the behavior observed in the last report? There, a 20 km tether cut at 0.5 and 1.0 km recoiled fully. When cut at 10 km, it only bounced up and down by about ½ km or so. For a 20 km tether, the various estimates of downfall are 0.6 and 0.8 km for complete downfall [free orbit (2) and D = r in (3)] and 0.07 for a long remnant [r = 10 km in (3)]. Our estimates appear somewhat conservative, though not excessively so. They could probably be somewhat refined by different or more sophisticated arguments. Perhaps, for instance, one could include "flyby" as well as "downfall": much of the tether actually bypasses the Shuttle, and as it falls down the gravity gradient potential on the other side it effectively pulls the remaining remnant behind it rather than simply vanishing from the equations as in the derivation of (3). Also, it would be interesting to conduct a series of simulations for remnants between 1 and 10 km to determine where the difference in behavior occurs.

2.4.5 Concluding Remarks -

The slack tether simulation program SLACK3 has been extended to include Shuttle thruster maneuvers. Simulations have been made incorporating thrusters for avoidance maneuvers. Simple brief bursts perpendicular to the orbit plane provide good initial avoidance, but prevention of long-term wrap-around will require more complex maneuvers. Design and simulation of these long-term avoidance maneuvers is an appropriate task for the next reporting period.

Several criteria for the impact of tether remnants on the Shuttle, based on energy arguments and similar general considerations, have been derived. The numerical results appear somewhat conservative when compared with the simulations reported in the previous quarterly report. The arguments leading to the criteria should be refined, and further simulations should be run to gain more precise knowledge of the transition from the complete downfall/flyby of short remnants to the bouncing behavior of long remnants.

Detailed theoretical (non-ball-and-spring) studies of the slack tether are now being carried out under separate contract. Appropriate results of these studies may be applied to specific cases of interest to the current contract.

2.5 Numerical Calculation Of The Electric Field Around An Electrodynamic Tether After Breakage

2.5.1 General -

In Quarterly Report #3 we described the development of a numerical program which solves Laplace's equation by the Liebmann net method. It was explained there that a geometrically varying grid was used to span a large region of space while allowing for a fine mesh spacing in the neighborhood of the end of the tether. The potential at the boundary of the grid was initialized by an analytical calculation of the field of a metallic prolate spheroid. This potential is expressed in terms of the Legendre function of the second kind of order one, $Q_1(\xi)$ where, as explained in Quarterly Report #2

$$Q_1 = \xi Q_0(\xi) - 1 \tag{1}$$

and

$$Q_0(\xi) = \ln\left(\frac{\xi + 1}{\xi - 1}\right) \tag{2}$$

The prolate spheroidal coordinate ξ is defined as

$$\xi = \frac{r_1 + r_2}{2c}. \tag{3}$$

The distances from the two focal points of the spheroid to any point in space, r_1 and r_2, are given in terms of the cartesian coordinates (x,y,z) by

$$r_1 = \sqrt{x^2 + y^2 + (z - c)^2} \tag{4a}$$

$$r_2 = \sqrt{x^2 + y^2 + (z+c)^2} \qquad (4b)$$

In this analysis as a result of axial symmetry we have replaced x and y by r, where:

$$r = \sqrt{x^2 + y^2} \qquad (5)$$

Thus

$$r_1 = \sqrt{r^2 + (z-c)^2} \qquad (6a)$$

$$r_2 = \sqrt{r^2 + (z+c)^2} \qquad (6b)$$

The numerical instability we reported in Quarterly Report #3 is a direct result of the square root operation. When r is small with respect to (z+c) or (z-c) then large round-off errors occur, and when z approaches c for large r equation (6a) causes large round-off errors.

When one term is much smaller than the other one can use the approximation

$$\sqrt{1 + \Delta} \simeq 1 + \frac{\Delta}{2} \qquad (7)$$

which is easily tested by squaring both sides of (7). If we substitute (6a) and (6b) into (2) we find that the argument of the log function becomes

$$\frac{r_1 + r_2 + 2c}{r_1 + r_2 - 2c} \qquad (8)$$

It is essential that care be taken to distinguish between the two cases $z > c$

and $z < c$ when using the approximation (7) with (8). Since r_1 and r_2 are positive numbers, in the limit as $r \to 0$, $\sqrt{(z-c)^2} \to |z-c|$. When $|z-c|$ is smaller than r we find that (7) results in

$$r_1 \simeq |z-c| + \frac{r^2}{2|z-c|} \tag{9}$$

When Δ in approximation (7) is not sufficiently small the error introduced by the approximation is unacceptably large. We have resolved this difficulty by replacing $\sqrt{1+x}$ with its Taylor series expansion.

If:

$$f = \sqrt{1+x} \tag{10}$$

then:

$$f = 1 + \frac{x}{2} - \frac{x^2}{8} + \frac{3}{8}\frac{x^3}{3!} - \frac{15}{16}\frac{x^4}{4!} + \ldots \tag{11}$$

This procedure accurately calculates $\sqrt{1+\Delta}$ even when $\Delta \to \frac{1}{2}$. In the following computation up to 30 terms in the series are used. This technique has completely removed the numerical instability from our computer model.

2.5.2 Computer Model Of The Electrodynamic Tether -

2.5.2.1 Grid Calculations -

The mesh box width $\Delta(n)$ are increased in a geometric progression such that

$$\Delta(n) = \alpha\, \Delta(n-1) \tag{12}$$

Thus n mesh boxes span a distance ℓ where

$$\ell = \Delta(1)\ \left[1 + \alpha + \alpha^2 + \alpha^3 + \ldots\ \alpha^{n-1}\right] \tag{13}$$

$$\ell = \Delta(1)\ \frac{\alpha^n - 1}{\alpha - 1} \tag{14}$$

To specify ℓ and n and calculate α would require the solution of a high order polynomial. We devised a simple numerical algorithm to calculate α given ℓ and n; such algorithm is implemented in this software code.

2.5.2.2 Contour Plots -

The grid chosen to model the tether covers a region ± 2 kilometers from the end of the tether in the z direction with a radius of 2000.001 meters. It is defined as an array of 91 x 161 points for a total of 14,400 mesh boxes. An equipotential contour plot of the analytically calculated field of a conducting prolate spheroid which models approximately the tether embedded in an axial field of 0.189 volt/m is shown in Figure 2.5.1. The region of the grid occupied by the tether was then set to zero and an index array which inhibits the calculation of potentials on the tether was initialized. A contour plot of the potentials calculated numerically by the Liebmann net method for the cylindrical

tether (1 mm radius and 20 km long) are plotted for the outermost 2 km of the tether in Figure 2.5.2. These two calculations are compared by superposing the two contour plots in Figure 2.5.3. Because of the nature of the high ratio geometric grid used for this calculation the shape of the field at the end of the tether is obscured in these plots. To resolve this difficulty the plots algorithm was modified to "zoom" in on the end of the tether. The first stage grid consisted of 90 x 160 mesh boxes, the second stage 50 x 80, the third stage 30 x 40 and the fourth 20 x 20. Thus the axial lengths of the grid in these four stages are 4 km, 1.9 m, 40 mm and finally 5 mm. Stages 2 through 4 are shown in Figure 2.5.4 through Figure 2.5.6.

2.5.3 Numerical Results -

This calculation was performed for the 28° orbit in which the 20 km tether, 2 mm in diameter, is exposed to a magnetically induced field of 0.189 v/meter (the worst case). The result of the calculation (vacuum case) are best shown in Figure 2.5.6. The voltage drop across the insulator, 2.5 mm from the tip of the tether (point B), is about 100 volts while the radial and the axial component of the electric field are respectively given by:

$$E_r = 330 \text{ Kvolt/m} \qquad (15)$$

$$E_z = 0$$

At the corner of the tether tip (point A), where we have assumed a squared edge and a flat top of the wire, the electric field is:

$$E_r = 1139 \text{ Kvolt/m} \qquad (16)$$

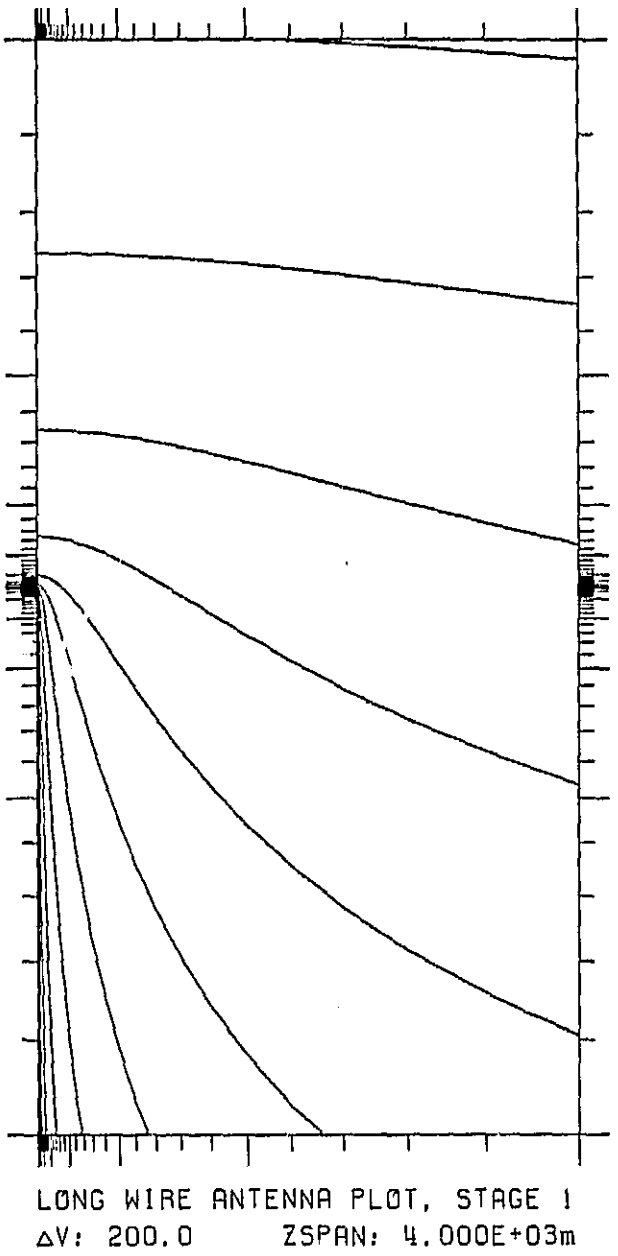

Figure 2.5.1. Analytically calculated electric potential (in vacuo) around a 20 km long tether, 2 mm in diameter cut at 20 km from the Shuttle. This Figure shows the last 2 km of tether (Stage 1).

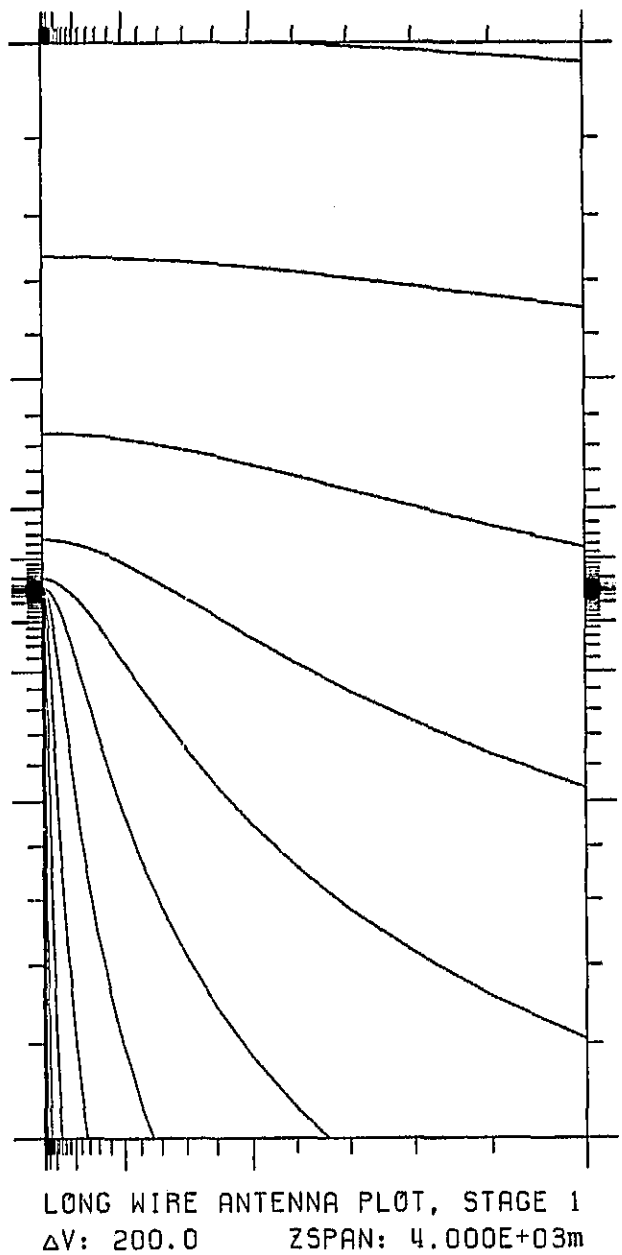

Figure 2.5.2. Numerically calculated electric potential (in vacuo) around a 20 km long tether, 2 mm in diameter cut at 20 km from the Shuttle. This Figure shows the last 2 km of tether (Stage 1).

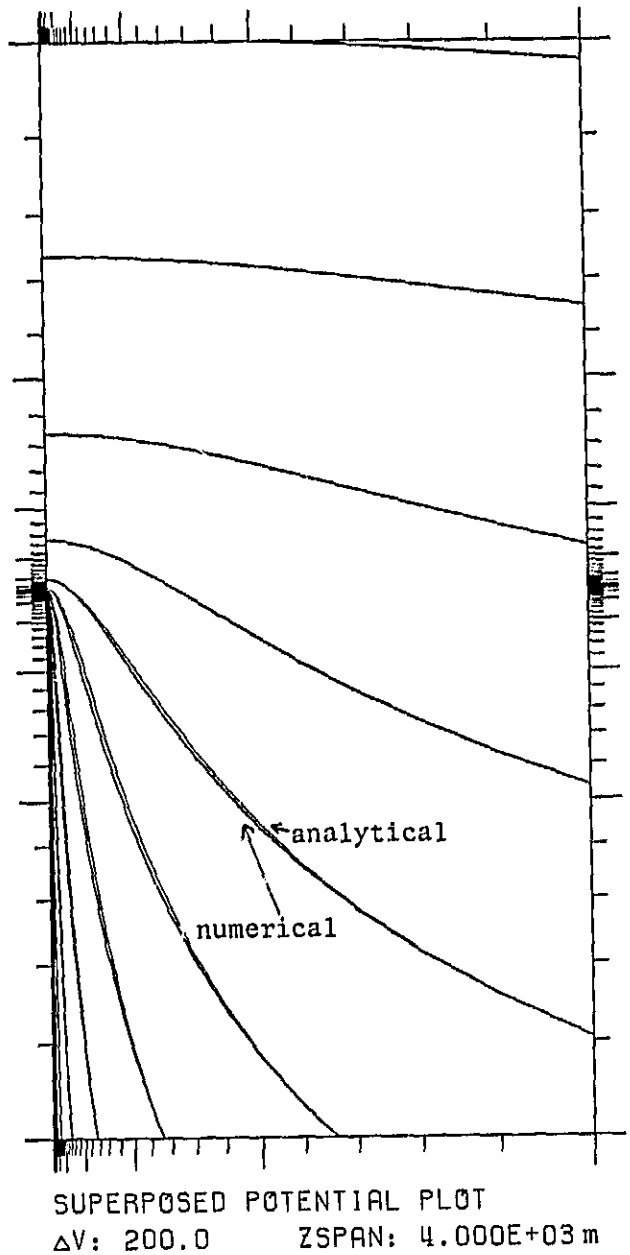

Figure 2.5.3. Comparison between analytically and numerically computed electric potentials around a 20 km long tether. This Figure is generated by superimposing Figure 2.5.1 and Figure 2.5.2.

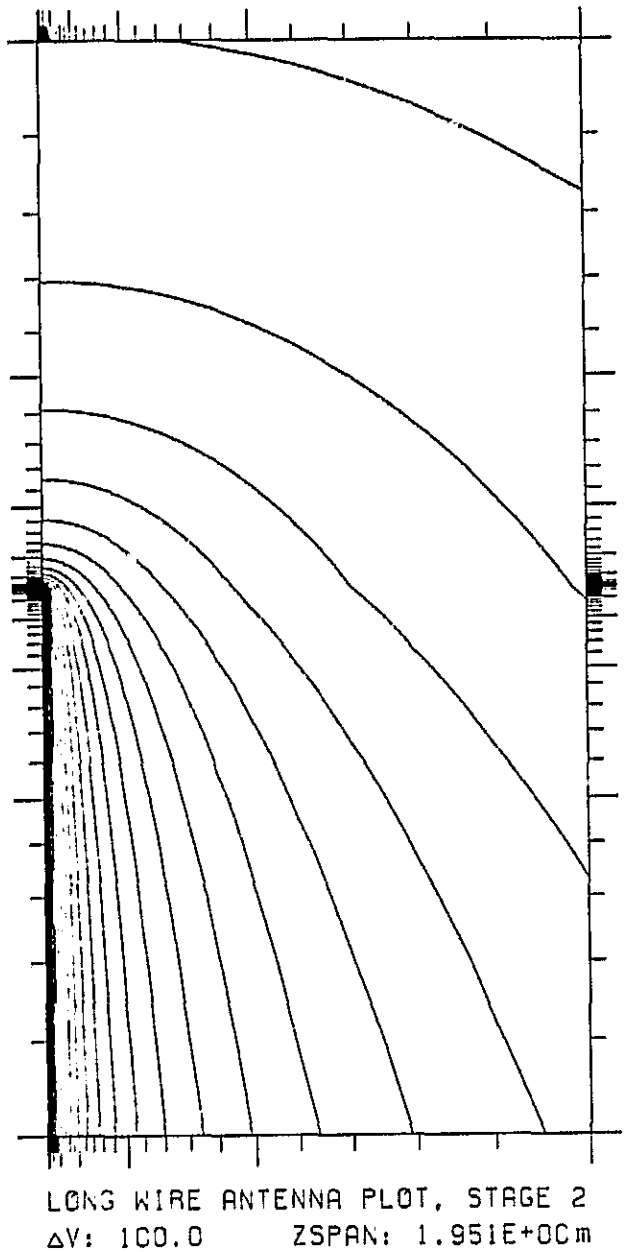

Figure 2.5.4. Zooming of the last 100 m of tether (Stage 2) with the same assumptions of Figure 2.5.2.

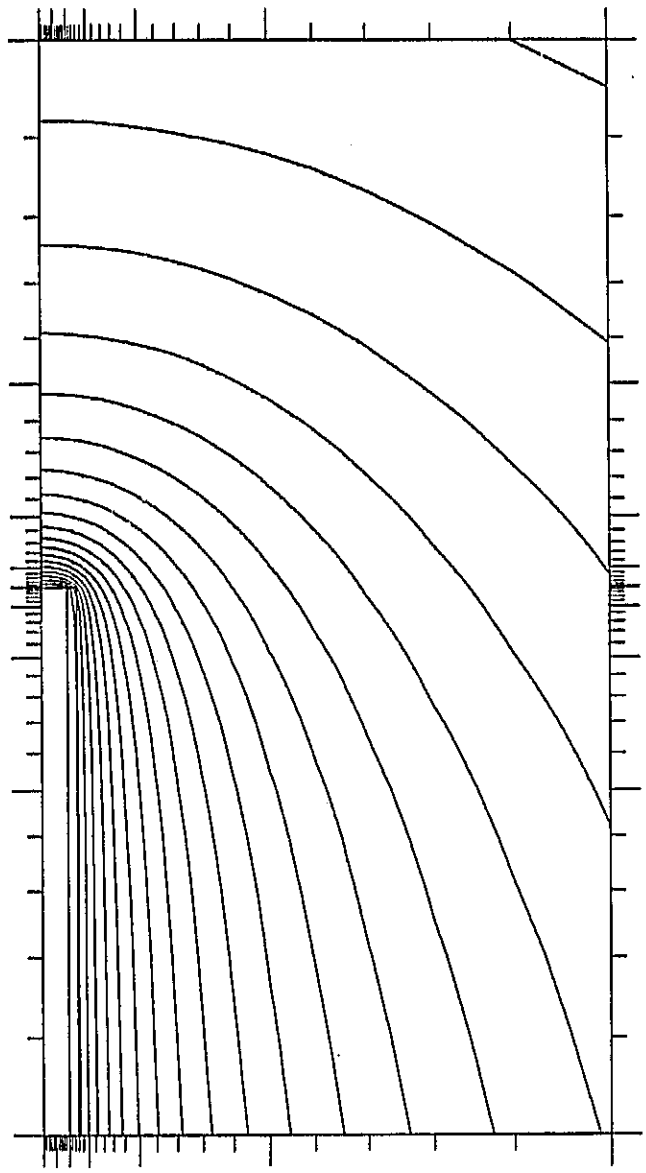

Figure 2.5.5. Zooming of the last 2.1 cm of tether (Stage 3) with the same assumptions of Figure 2.5.2.

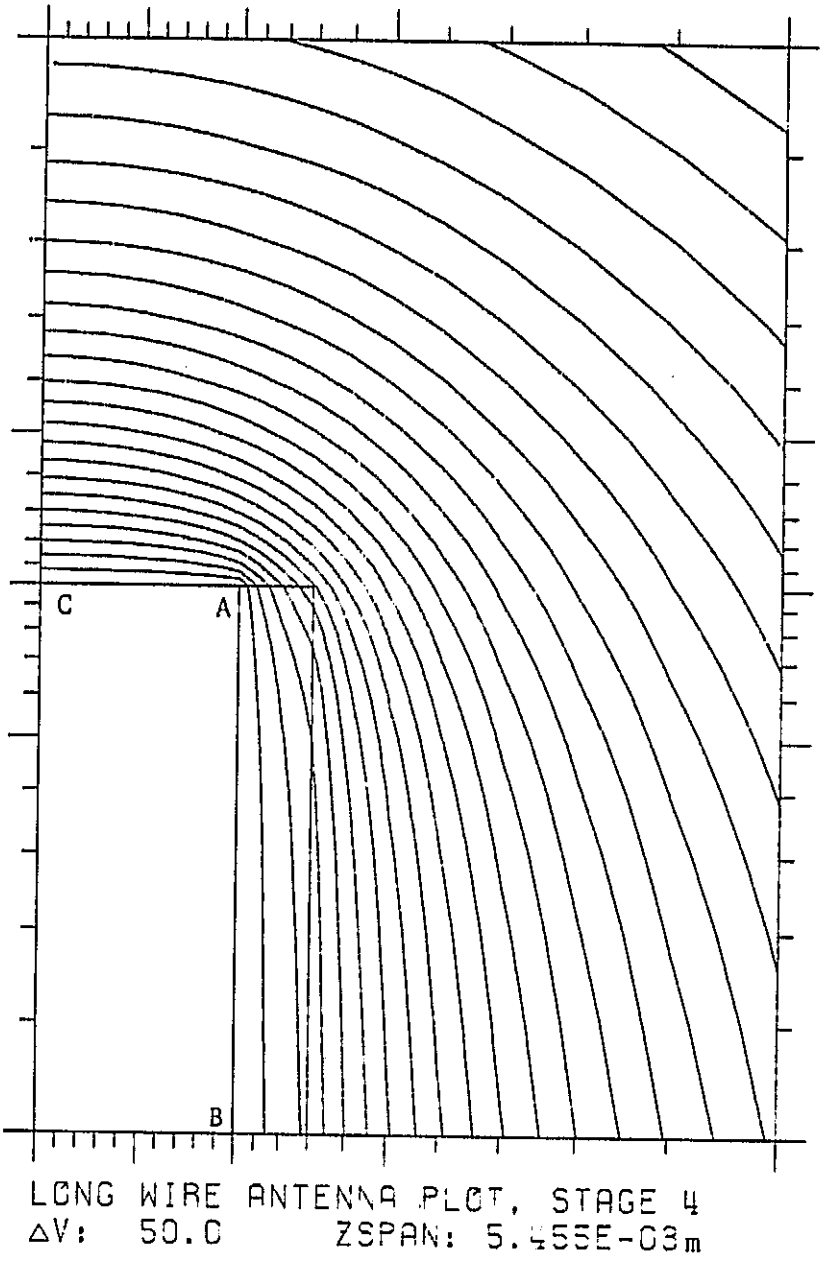

Figure 2.5.6. Zooming of the last 2.7 mm of tether (Stage 4) with the same assumptions of Figure 2.5.2.

$$E_z = 1350 \text{ Kvolt/m}$$

These are also the maximum values for the electric field in the case under investigation. At the very tip of the tether (point C), where the tether is assumed to be flat, the electric field is:

$$E_r = 0 \tag{17}$$

$$E_z = 700 \text{ Kvolt/m}$$

This computation takes into account the effect produced by the insulator around the conducting wire. The insulator characteristics for the TSS first mission, provided by MMA, are as follows:

insulator thickness $\simeq$ 0.36 mm
dielectric constant = 2.1 (18)
dielectric strength = 1200 volt/mil = 47 Kvolt/mm = 47000 Kvolt/m

It is therefore interesting to notice that (in vacuo) the dielectric strength of the insulator is never exceeded even after the tether breakage. It is also interesting to see how the value of the electric field computed by this high fidelity model compares to the simplified single-dimensional computation performed in Quarterly Report #1. In that Quarterly Report we preliminarly computed the electric field at point C in Figure 2.5.6 assuming that the tether was a prolate spheroid. The prolate spheroid however has a too small radius of curvature at the tip so that we corrected that value by a factor of 2×10^7 that relates the radius of curvature of the prolate spheroid to that of a tether with a semispherical tip. The result was as follows:

$$E_z = 4.5 \times 10^{12}/20^7 = 225 \text{ Kvolt/m} \qquad (19)$$

This value is of the same order of magnitude of that computed with the high fidelity model.

2.6 Preliminary Estimation Of The Electrodynamic Hazards Due To The Breakage Of A Tether Embedded In A Plasma

2.6.1 Introductory Remarks -

A preliminary analysis is underway of the mechanisms by which a Shuttle-borne long electrodynamic tether, broken at a certain point along its deployed length, may produce harmful effects.

2.6.2 Effects Of Break -

Assuming a break occurs near the Shuttle, two of the possible hazardous effects are the following:

a) Appearance of high voltage across the break, which can accelerate electrons toward the Shuttle, so that the Shuttle is bombarded by high-energy electrons.

b) Arc drawn in vacuum between separating contacts extinguishes abruptly, radiating a pulse of electromagnetic energy that may be powerful enough to produce EMP-type effects.

We consider, first, effect (a), then (b).

2.6.3 High Voltage Across Break -

When a circuit carrying current is interrupted, either intentionally by a switch or inadvertently by a break as in the present case, an arc is drawn between the separating contacts (Cobine, 1958). The present problem represents the case of a vacuum arc (Lafferty, 1980). As the contacts separate and the gap length increases, a point is reached where the available voltage is insufficient to sustain the arc and the arc is extinguished. If there were no inductance in the external circuit, then at this gap length the post-extinction voltage across the gap would rise from its normal operating value (vicinity of 20V) to the circuit driving voltage or e.m.f. (Cobine, 1958), which is about 4 kV in the case of the electrodynamic tether.

If there is inductance in the circuit, then the current continues to flow while the contacts continue to separate further. At some (presently unknown) point the arc extinguishes, and the voltage across the gap simultaneously rises to its "extinguishing" value, which depends on the arc current-voltage characteristic. The extinguishing voltage can be much larger than the circuit driving voltage (Cobine, 1958).

In addition, because of stray capacitance in the vicinity of the arc, the interruption can give rise to high transient voltages across the contacts. This is because the magnetic energy stored ($LI^2/2$, where L is the inductance and I is the current) flows into the capacitance in the form of electric energy ($CV^2/2$, where C is the capacitance and V is the resulting transient voltage). This energy subsequently oscillates between the two forms. If all the energy is transferred in this way (no losses) then, equating the two energies, the resulting voltage across the capacitance (and therefore across the contacts) would be:

$$V = I\ (L/C)^{1/2}$$

where $(L/C)^{1/2}$ is the "surge impedance," and I is the current flowing prior to interruption. Thus, the voltage can be large independently of the driving voltage if the surge impedance is large. There is also a resonant frequency f determined by the relation:

$$2\pi f = (LC)^{-1/2}$$

Hence a small stray capacitance results in a large surge voltage, and an oscillation at high frequency.

We need therefore to address the problem of the evaluation of how much voltage can appear across the contacts and thus give rise to accelerated electrons that can bombard the Shuttle. Some rough numerical estimates will be given later.

2.6.4 Pulse Of Electromagnetic Energy -

As the contact separation increases, the arc (drawn in vacuum) grows in length. At some point (not presently known) the arc extinguishes. The interruption of current results in electromagnetic radiation, the properties of which depend on the details of the time and space behavior of the current. Rough estimates of this radiation pulse are given in the next section.

2.6.5 Numerical Estimates Of Bombardment -

Assume the following parameters:

Tether length = 2×10^4 m

Conducting wire radius: 0.5 mm (r_1)

Outer radius of wire insulation: 0.75 mm (r_2)

Inductance of 20 km tether: 0.012 h (L)

Capacitance of 20 km wire (with respect to r_2): 2.8×10^{-6} F

Tether current: 1A

Break separation velocity: 4.2 m/s

Electron conical beam semi-angle: 30 degrees

We may obtain estimates of the surge impedance (L/C) and therefore of gap voltage if we know the values of C and L. Since the problem is a dynamic one involving not only the arc itself but also the tether with finite propagation times and attenuations of waves moving along it, the appropriate effective values of L and C are difficult to estimate. One extreme limit is obtained by treating the whole tether as a lumped circuit element with L = 0.012 h and C = 2.8×10^{-6} F. This gives an underestimate, namely, a surge impedance of 65 Ω, and therefore a low surge voltage of only 65 V.

At the other extreme, an overestimate is afforded by taking the capacitance as that of the wire tip, namely, 5.6×10^{-14} F, while retaining the whole tether inductance, 0.012 h. This gives a surge impedance and voltage of 4.6×10^5 Ω and 460 kV. While admittedly this overestimate of V results from using too large a value for inductance, namely, the whole-tether inductance, it is useful as a worst-case since the appropriate value of inductance is unknown. A reasonable compromise value for V may be obtained as the geometric mean between the lower limit, 65 V, and the upper limit, 460 kV, namely, 5500 V. (Note that

this value is comparable with the normal driving voltage, 4000 V.)

2.6.6 Bombardment Of The Shuttle -

The time during which electrons would be accelerated at this voltage is given by 1/2 of the period of the high-frequency oscillation, namely, $\pi(LC)^{1/2}$, or 80 ns. During this time period, 5-kev electrons, moving with velocity 4.2×10^9 cm/s can travel 3.4 m. However, henceforth we will assume a distance of the order of 1 meter.

To estimate the particle energy flux onto the Shuttle, we assume that 1 ampere of electrons, confined to a conical beam of semi-angle 30°, strikes the Shuttle one meter away. The angle 30° is characteristic of beams emitted from the cathode spots in vacuum arcs (Reece, 1963). Assuming that one ampere of 5-kev electrons hits one square meter of Shuttle surface, we obtain 6.25×10^{14} electrons/cm^2/s. This is orders of magnitude larger than the fluxes of radiation-belt electrons of comparable energy. Hence, some damage may be done by the pulse, but this needs yet to be quantified.

2.6.7 Numerical Estimates Of EMP -

The electromagnetic radiation depends on the details of the time and space behavior of the current. In particular, the current distribution in the arc is of interest, but this is an unsolved problem to date (see e.g. Lafferty, 1980). For example, a conical jet of metallic vapor is emitted from a cathode spot. Electrons are also emitted by thermoionic field emission. Avalanches occur, producing ionization of the metal. Some of the ions, but not all, bombard the cathode releasing more electrons. The dense metallic vapor moves at high speed, dragging along the ions. At some point, the jet has expanded until it is so

rarefied that the ion mean free paths are long and the ions are no longer dragged along. Thus, the plasma is highly collision-dominated near the cathode, and becomes collisionless downstream. This transition between collision-dominated and collisionless regimes is partly responsible for the difficulties of modeling this phenomenon.

However, we will make a rough estimate, as follows. Assume that the arc current is one ampere, and that it is one meter in length before it extinguishes. Assume that the extinction of current I occurs over a period of 10-100 ns (Farrall, in Lafferty, 1980, p. 194-5). We will use a dipole approximation. Assume the length of current is h = 1m. The radiation electric field at a distance of r may be approximated by

$$E = \frac{h\, dI/dt}{4\pi\epsilon C^2 r}$$

If I changes by 1 A in 10 ns, $dI/dt = 10^8$ A/s. Using this, together with h = 1m, $\epsilon = 8.85 \times 10^{-12}$ F/m, $C = 3 \times 10^8$ m/s, we obtain

$$E \simeq 10/r \ \text{(V/m)}$$

Hence, at r = 1 m the induced electric field is about 10 V/m, i.e., a weak field. This may be an indication that the EMP-type threat is weak. However, the model is too crude, and needs to be examined more carefully.

It should be noted that the energetic electrons discussed above may liberate x-rays due to the surface bombardment. These x-rays may possibly be a hazard that warrants further examination.

3.0 PROBLEMS ENCOUNTERED DURING REPORTING PERIOD

None.

4.0 ACTIVITY PLANNED FOR THE NEXT REPORTING PERIOD

The simulation activity on the satellite's rotational dynamics will continue by performing retrieval simulations with and without out-of-plane tether libration and thruster libration control. An investigation of the coupling between thrusters' activation and tether dynamics, in the case of constant tether length, will be initiated.

The analysis of Shuttle's maneuvers in order to avoid the recoiling tether after its severance will be further developed. Simulation of most important cases, as agreed upon by NASA/MSFC experts, will be carried out. Optional solutions to minimize dangers to the Orbiter will be looked for.

The study of electrodynamic hazards caused by the breakage of the TSS electrodynamic tether embedded in a plasma will continue by improving on the understanding of the most likely consequences.